ELECTROMAGNETIC TRANSMISSION THROUGH DIELECTRIC SHEETS

DISSERTATION

Presented in Partial Fulfillment of the Requirements for the Degree Doctor of Philosophy in the Graduate School of The Ohio State University

By

JACK HUBERT RICHMOND, B. S., M. Sc.

*****

The Ohio State University
1955

Approved by:

T E Tice

Adviser
Department of Electrical Engineering

ACKNOWLEDGMENT

The suggestions and encouragement of my adviser, Professor T. E. Tice, are gratefully acknowledged. Valuable discussions with Professors R. L. Cosgriff, R. G. Kouyoumjian, and C. T. Tai are greatly appreciated.

The research reported herein was sponsored in part by the Air Research and Development Command, Wright-Patterson Air Force Base, Ohio, under a contract with The Ohio State University Research Foundation.

PREFACE

Radar antennas on aircraft and missiles must be covered with dielectric shells or radomes for streamlining. The radome introduces errors in the indicated target position, and must be designed to minimize such errors. While the optical approximations generally employed in radome design may be satisfactory for large, well rounded radomes, they are often inadequate for small, highly streamlined shapes. Improved approximate methods of analysis are needed to replace the slow, costly, cut-and-try methods now in use for such radomes.

In seeking an improved design procedure, maximum use should be made of any available experimental measurements. Although the radome is assumed to be in the design stage and not yet constructed, the radar antenna to be used is often available. In Chapter II various techniques are investigated for use in the accurate measurement of the electromagnetic fields near an antenna. The properties of a coherent detector are found to be particularly useful. A balanced coherent detector is unusually sensitive and permits measurement of time-quadrature components as well as automatic phase measurements.

The scattering method of measuring electric field distributions is capable of unusually high accuracy. To simplify the scattering measurements and at the same time increase the sensitivity and accuracy, a new technique was developed employing a modulated scatterer. A comparison of various probes led to the development of an open-

ended waveguide probe which is of simple construction, has an aperture small enough to measure complicated field distributions, and has proven sufficiently accurate for many measurements.

In radome design it is frequently necessary to calculate the radiation pattern of an antenna covered with a radome. The surface integrations usually involved are considered in Chapter III. It is found that the calculations are simplified if a plane reference surface is chosen. The surface integration may be further simplified to a line integration if the electric fields are separable. The numerical work may be reduced with little loss in accuracy by replacing the continuous field distribution near the antenna with an array of point sources spaced nearly one-half wavelength apart.

Conventional radome analysis methods require a mathematical description of transmission through a radome located in the Fresnel zone of an antenna. By an application of the reciprocity theorem, this problem is replaced in Chapter IV by the simpler problem of transmission of a plane wave through the radome from a distant source. A particularly simple result is obtained by this approach for transmission through an infinite plane dielectric sheet inclined at some angle from the antenna aperture. If interaction between the antenna and the sheet is negligible, the radiation pattern with the sheet is merely the unperturbed pattern multiplied by the plane-wave plane-sheet transmission coefficient. This has been verified experimentally.

The theory has also been applied to transmission through finite plane sheets. Simplified approximate calculations have been carried out and yielded satisfactory agreement with measured data. It is

felt that these results justify future attempts to apply the theory and techniques to the problems of transmission through curved dielectric sheets and radomes.

CONTENTS

ELECTROMAGNETIC TRANSMISSION THROUGH DIELECTRIC SHEETS

I. INTRODUCTION

Radar antennas on aircraft, ships, and even in many ground installations must be covered with a dome to protect the antenna from wind and moisture. An excellent introduction to the theory of radar antenna domes, or radomes, is given in reference (1). A radome must be as transparent as possible to electromagnetic waves at the radar frequency. Radomes present a number of electromagnetic problems, and these may be especially difficult in radar systems which indicate the angular position of a target, as contrasted with ranging radar. A radar system which performs satisfactorily before the radome is installed may show a reduction in range and a decreased accuracy with the radome in place. These effects are introduced through antenna pattern distortion caused by the radome. The pattern distortion produced by a radome may include the following types: attenuation, beam tilt, and change in beam width. The angular difference between the apparent target position indicated by the radar and the line of sight is called the boresight error. Radomes for systems which aim guns or guide missiles must introduce a minimum boresight error.

The electrical design of a radome includes the specification of the dielectric constant and loss tangent of the material and the thickness and shape of the radome. The choice of dielectric constant

and loss tangent is limited by the available materials which have properties suitable for radome use. In some applications radomes are subjected to temperature extremes, large wind loads, and great acceleration forces. The choice of radome shape is also limited, especially in high speed aircraft and missiles, by aerodynamic considerations. Whereas a hemispherical radome is usually the best electrical design, a highly streamlined shape is preferred to reduce wind resistance and rain erosion.

An exact solution for the fields of an antenna enclosed in a radome is available only for the simplest case: a short dipole in a spherical radome (2). Even in this case difficulty is experienced in obtaining useful information from the solution. It is found that the functions involved are not sufficiently well tabulated. Furthermore, the infinite series which express the solution are slowly convergent. These problems would also accompany the select few remaining radome shapes which fit coordinate systems in which the wave equation is separable, and which therefore would permit rigorous analysis.

The radome design problem is complicated by the fact that the antenna usually must aim in various directions through the radome to keep a moving target in view. In addition, some type of scanning such as conical scanning is employed to obtain accurate direction information while using a small, broad-beam antenna. One might consider calibrating the radome and using automatic equipment to make corrections for the radome errors. While this is possible, it would

be an unsatisfactory solution to the radome problem in view of the size and weight of the extra equipment required. Furthermore, the reliability of the system would be reduced by the possibility of failure of the additional components.

Approximate methods must therefore be employed in the analysis and design of radomes. Large, well rounded radomes are successfully analyzed using approximations from physical optics. The radome may be approximated by a number of plane dielectric sheets tangent to the actual radome. Plane-wave plane-sheet theory may then be used to design radomes for high transmission coefficient, low reflection coefficient, constant insertion phase delay, and other desirable properties. The radome may be thought of as a lens, and lens formulas are sometimes applied. These approximate methods, however, are found to give only qualitative results when applied to small, highly streamlined radomes. New approaches and more exact analyses are needed to replace the slow, costly, empirical, cut-and-try methods in use today.

The development of an approximate analytical procedure suitable for streamlined radomes is the subject of this dissertation. To promote an understanding of the phenomena involved, and to avoid the necessity for large high-speed computers in the investigation, the radome problem was simplified by considering plane dielectric sheets rather than actual curved radomes. It is felt that the methods used with finite plane sheets will be found useful with streamlined radomes, especially since it has been observed that the fields near the

edge of a plane sheet resemble those near the sharp nose of a radome.

Since a large number of measurements of fields near antennas was required in this study, it was found necessary to investigate techniques for accurate probing of fields and for sensitive detection of microwave signals. As a number of antenna radiation patterns had to be computed from given near-field distributions, a simplified computation procedure was developed. The following chapters will consider techniques for measuring microwave field distributions and for calculating antenna field patterns. The results will then be utilized in an analysis of antenna pattern distortion by infinite and finite dielectric sheets.

REFERENCES

1. W. M. Cady, M. B. Karelitz, and L. A. Turner, "Radar Scanners and Radomes", McGraw-Hill Book Co., New York, 1948.

2. T. E. Tice and J. E. Adney, "Transmission through a Dielectric Spherical Shell", Technical Report 531-3, Antenna Laboratory, The Ohio State University Research Foundation; August 1, 1953.

II. MEASUREMENT OF ELECTROMAGNETIC FIELDS NEAR ANTENNAS

A. A BALANCED COHERENT DETECTOR FOR MICROWAVE MEASUREMENTS

1. INTRODUCTION

The far-field calculations discussed in Chapters III and IV require a knowledge of the fields on some surface enclosing a transmitting antenna. Scattering and probing methods for measuring such fields are investigated in Sections B and C of the present chapter. The high sensitivity available with coherent detection permits the use of smaller, more accurate probes and scatterers. A balanced coherent detector permits the direct measurement of the time-quadrature components which are found to be convenient in certain far-field calculations in Chapter III. The properties of the balanced coherent detector are employed in Section B of the present chapter in the development of a modulated scattering system. For these reasons the following study was made of coherent detection.

Let E denote some microwave signal or electric field intensity to be measured, and let $|E|$ and α denote its amplitude and phase. E may be a function of the position of a probe exploring the fields near a transmitting antenna. For convenience in making calculations it is often desirable to record the time-quadrature components $|E| \cos\alpha$ and $|E| \sin\alpha$. These are also called the real and imaginary components and are denoted R(E) and I(E), respectively. It is found possible to make direct measurements of R(E) and I(E) with equipment which is less elaborate than that required for direct measurements of amplitude and phase.

2. THEORY

Figure 2.1 illustrates the equipment used for measuring R(E) and I(E). The detector is commonly referred to as a coherent or synchronous detector (1). Synchronous detection has been proposed and analyzed in the past (2), but its use at microwave frequencies has involved difficulties which have been overcome only recently with the development of nonreciprocal waveguide sections and waveguide modulation techniques.

The receiver is used at a frequency of 9400 mc. Two type 821 Sperry bolometers are used as the detecting elements. An unmodulated signal A of constant phase and amplitude is applied to the bolometers directly from the klystron. In addition a test signal E, amplitude-modulated at some audio frequency (1000 cps), is applied. The bolometers are connected to the collinear arms of a hybrid junction, and signals A and E arrive through the two orthogonal arms. Tuning is provided in one collinear arm to achieve maximum isolation between signals A and E. Because of the properties of the hybrid junction, the total signals arriving at bolometers 1 and 2 are, respectively,

$$E_1 = A + E, \tag{2.1a}$$

and

$$E_2 = A - E. \tag{2.1b}$$

If A is taken as a phase reference, eqs. 2.1 become

$$E_1 = A + |E| \cos \alpha + j\, |E| \sin \alpha, \tag{2.2a}$$

and

$$E_2 = A - |E| \cos \alpha - j\, |E| \sin \alpha. \tag{2.2b}$$

The output voltages V_1 and V_2 of bolometers 1 and 2 are proportional

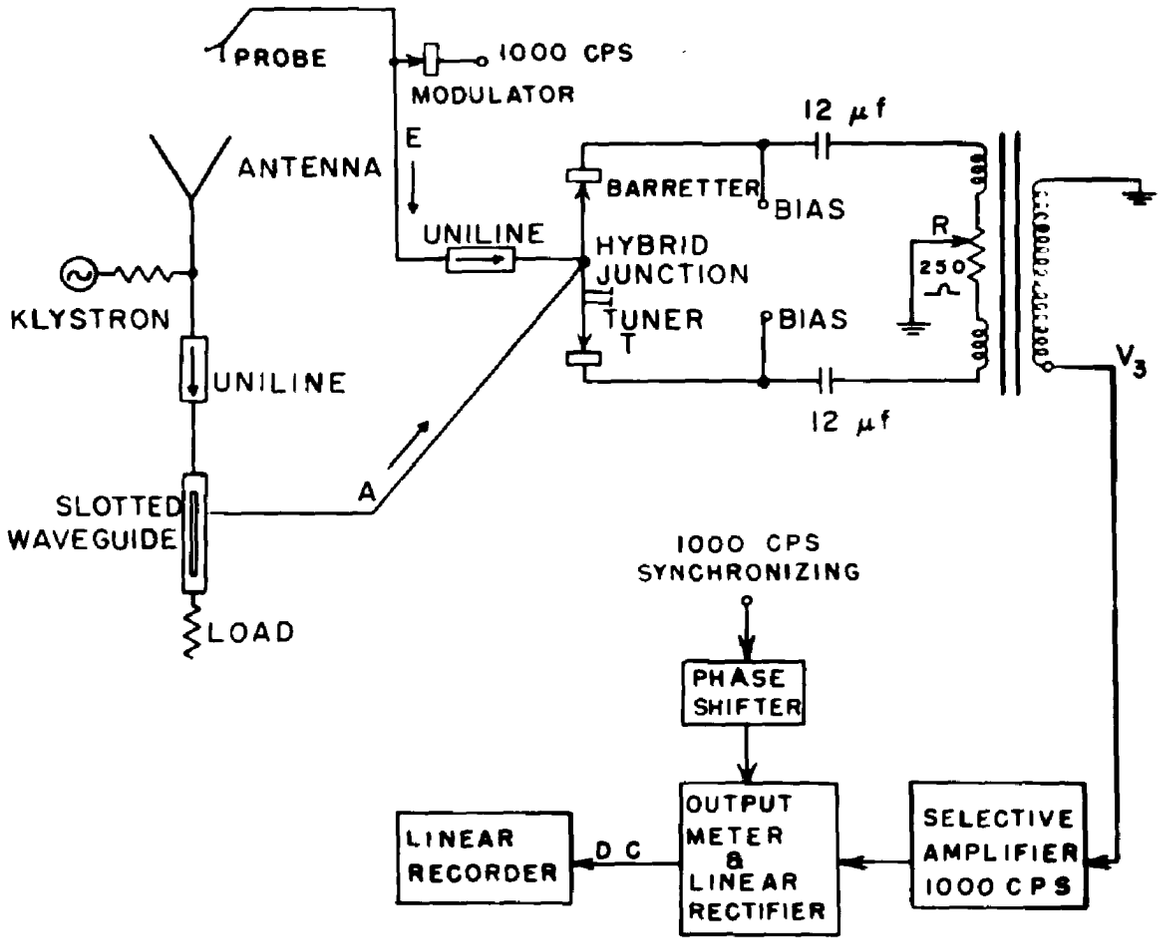

Plate I

Fig. 2.1. Equipment for measuring the real and imaginary components of a microwave signal.

to the squares of the amplitudes of E_1 and E_2, respectively. The constant of proportionality is of no concern in this discussion and will be omitted. Thus,

$$V_1 = (A + |E| \cos \alpha)^2 + (|E| \sin \alpha)^2, \qquad (2.3a)$$

and $$V_2 = (A - |E| \cos \alpha)^2 + (|E| \sin \alpha)^2. \quad (2.3b)$$

An audio transformer takes the difference between V_1 and V_2, yielding

$$V_3 = 4 A |E| \cos \alpha. \quad (2.4)$$

Thus, since A is held constant, V_3 is proportional to R(E).

Now, a similar detector could be added alongside the one shown in Fig. 2.1 and adjusted to provide an output signal 4 A |E| sin α proportional to I(E). This could readily be accomplished by applying signals A and E as before but with a phase shift of 90° inserted in the path of A. At present, however, this additional complexity of equipment is avoided at the cost of an increase in operating time. This is done by conducting each experiment twice, recording R(E) the first time, shifting signal A through 90° in phase with the slotted waveguide shown in Fig. 2.1, and finally recording I(E).

The reference signal A may be thought of as a local oscillator signal in comparing coherent detection with superheterodyne detection. However, since the reference signal comes from the same source as the test signal E, there is no problem of frequency stabilization to maintain a constant difference frequency as in a conventional superheterodyne receiver. The necessity for a reference signal direct from the transmitter limits the use of coherent detection to laboratory measurements.

3. EQUIPMENT AND ADJUSTMENT

The Uniline is a nonreciprocal waveguide attenuator which allows transmission in the forward direction with little loss but

provides a large attenuation for energy traveling in the reverse direction. The Unilines shown in Fig. 2.1 help isolate the klystron from variations in load impedance and provide extra isolation between signal A and the modulator.

The modulator in use consists of a 1N23 crystal in a tunable detector mount. An audio modulating signal of about three volts at 1000 cps is applied to the crystal, and the resulting variations in crystal impedance produce amplitude modulation on the microwave signal traveling through the waveguide. As compared with square-wave modulation of the klystron, crystal modulation involves a loss of 3 or 4 db of sensitivity because of incomplete modulation. However, it is desirable that the reference signal be unmodulated; hence, klystron modulation would not be suitable. If the reference signal were modulated, the measurement of small test signals would be interfered with by a residual output signal present in the receiver due to imperfect audio nulling. A simple audio nulling circuit (merely potentiometer R) is satisfactory if the reference signal is unmodulated.

The selective amplifier (3), built at the Antenna Laboratory, has a pass band of 4 cps centered at 1000 cps. The linear rectifier to be used depends on factors such as the dynamic range required. A chopper rectifier, synchronized with a properly phased signal from the modulator, should be satisfactory. A type 1N34 germanium diode is in use at present. The diode is operated at a signal level large enough to obtain linear response.

Two nulling operations are involved in adjusting the equipment. Signal A is disconnected from the hybrid junction, and a test signal E of about 1 mw is applied. A detector is connected to the hybrid junction at the terminal where signal A was removed. Tuner T is then adjusted for a null indication at the detector. A second nulling operation is now performed by adjusting potentiometer R for a minimum indication at the detector.

4. PERFORMANCE

As a test of accuracy, the equipment was used to measure known fields in a waveguide. The antenna shown in Fig. 2.1 was replaced with a slotted waveguide. A probe moving along the waveguide axis extracted a test signal E. Measurements were taken with the slotted waveguide terminated with a metal reflector and then with a matched load. The results are shown in Fig. 2.2. In both cases, theory indicates that R(E) should be a sinusoidal function of distance x along the waveguide axis. As is evident in the figures, excellent agreement was obtained between the theoretical and measured functions. Any slight disagreement is as likely to be caused by an imperfect slotted waveguide or termination as by any inherent defect in the detector. These measurements were repeated with equally good results at signal levels up to 1 mw with a reference power of 1 mw.

The sensitivity of the equipment with a reference signal of 10 mw was measured as - 125 dbw at 9400 mc. That is, a test signal power of -125 dbw was required to raise the receiver output by 3 db

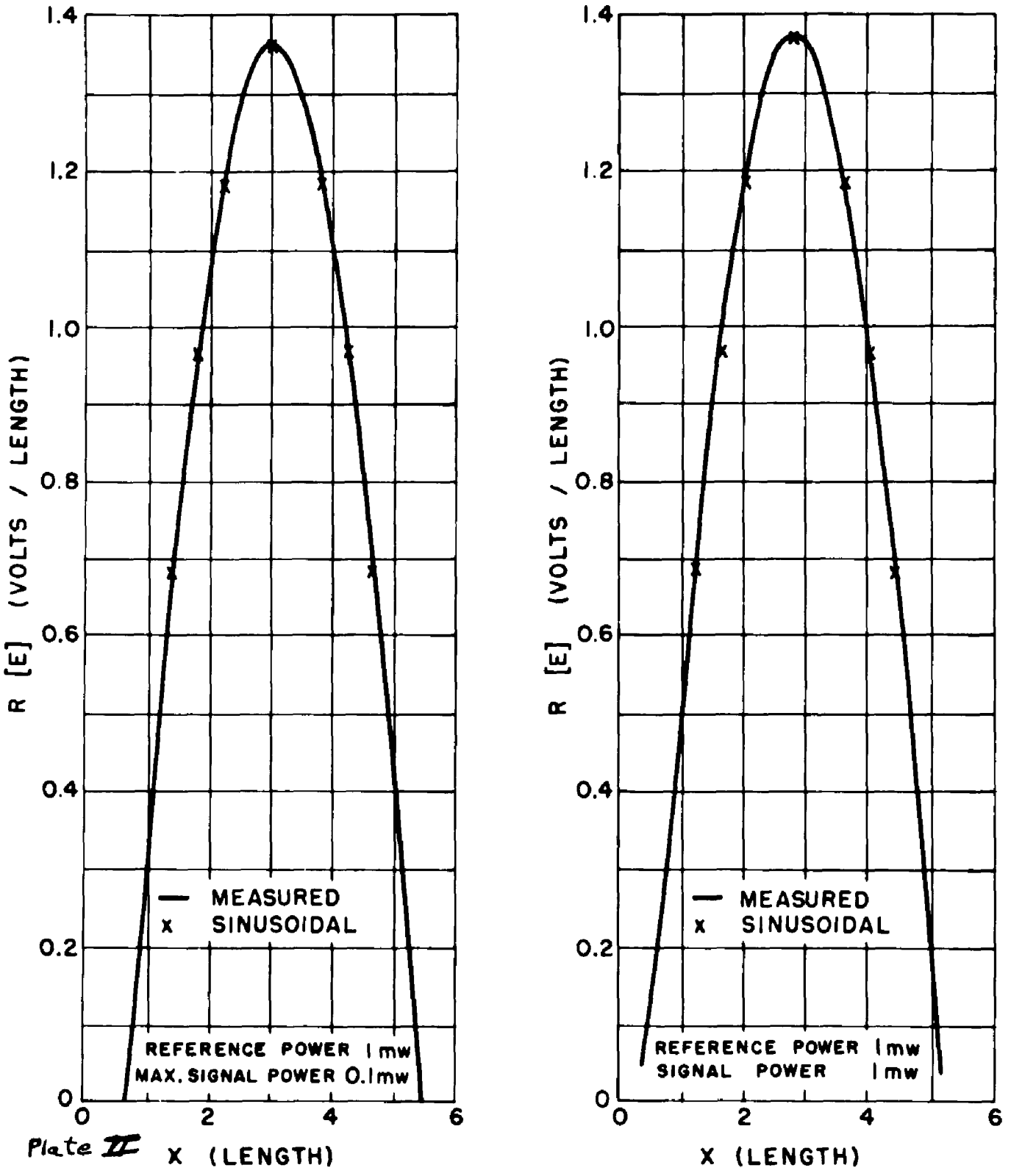

Fig. 2.2. Real component of electric field intensity in shorted waveguide (left) and matched waveguide (right).

over the output noise level observed in the absence of any test signal. This could no doubt be improved, if desired, by using a more efficient modulator, and adjusting the bolometer bias current to the optimum value. A bias current of 5 ma was used for each bolometer.

The measurements listed in Table I show that the output noise of the receiver increases somewhat as the bolometer bias current is increased, but is quite insensitive to the reference signal level.

TABLE I

Average Receiver Noise Output as a Function of Bias Current and Reference Power Level in the Absence of a Test Signal

BIAS CURRENT (ma)	REFERENCE POWER (mw)	NOISE OUTPUT (v)
0	0	0.33
5	0	1.00
5	10	1.18

Equation 2.4 indicates that the output signal should be proportional to the reference level A for a given test signal E with a given phase angle. This was found to be accurate as long as A was stronger than E. This condition is easily satisfied in practice.

It was found that crystals performed as well as bolometers in the coherent detector. The waveguide field measurements shown in Fig. 2.2 were repeated using 1N23 crystals with equally good results. The sensitivity of the coherent detector using crystals was found to be -123 dbw at 9400 mc. This measurement was made with the reference

signal adjusted to the optimum level, which was found to be -36 dbw at each crystal.

B. A MODULATED SCATTERING TECHNIQUE FOR MEASUREMENT OF FIELD DISTRIBUTIONS

1. INTRODUCTION

The analysis of microwave transmission through dielectric sheets developed in Chapter IV requires a knowledge of the electric field intensity distribution near a transmitting antenna. Electric field intensity is generally measured by inserting a small test antenna in the field and observing the voltage V induced at its terminals. Let S denote a surface which encloses the probe as in Fig. 2.3. Let E

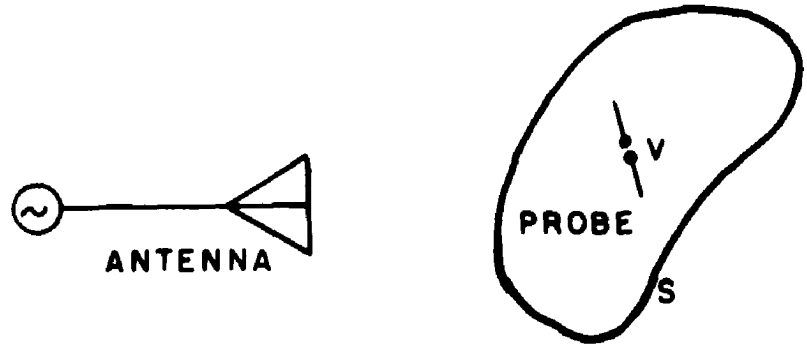

Plate III

Fig. 2.3. The fields of a transmitting antenna being measured with a probe surrounded by a reference surface S.

and H denote the electric and magnetic field intensities set up on S by the transmitting antenna in the absence of the probe. If the probe, when functioning as a transmitter, sets up fields E_1 and H_1 on S in the presence of the antenna, we may define electric and

magnetic currents J and K on S which are equivalent to the probe:

$$J = n \times H_1, \tag{2.5a}$$

and

$$K = E_1 \times n, \tag{2.5b}$$

where n is the outward unit normal on S. It has been shown by Kouyoumjian (4) that

$$V = C \iint_S (J \cdot E - K \cdot H)\, ds, \tag{2.6}$$

where C is a constant determined by certain impedances and the strength of the sources used and will be omitted in the following discussion. If the probe is a thin linear dipole, and if surface S is chosen to coincide with the dipole surface, eq. 2.6 reduces to

$$V = \int I \cdot E\, dz = \int I(z)\, E_z(y,z)\, dz, \tag{2.7}$$

where z denotes distance along the dipole axis, I(z) is the current distribution on the dipole when functioning as a transmitter, and E_z is the component of E tangential to the dipole. If the dipole is sufficiently short so that E_z is constant both in phase and amplitude along the dipole,

$$V = E_z(y_o, z_o) \int I(z)\, dz, \tag{2.8}$$

where y_o and z_o are the coordinates of the center of the dipole. Thus, a short thin linear dipole would accurately indicate the incident electric field intensity component parallel to the dipole.

It is apparent from eq. 2.6 that in general a probe does not indicate the field intensity at a point, but rather some weighted average of the fields. As is discussed in Chapter III, the fields of certain antennas are separable in rectangular coordinates to a good approximation; that is,

$$E_z(y,z) = Y(y)\, Z(z). \tag{2.9}$$

In this case eq. 2.7 becomes

$$V = Y(y) \int I(z)\, Z(z)\, dz. \tag{2.10}$$

Thus, in separable fields the finite dipole accurately indicates the electric field distribution on a path parallel to the y-axis, but indicates a weighted average of the electric field distribution on a path parallel to the dipole axis. Unfortunately, the properties of a dipole are considerably altered by the presence of the cable which must be used to deliver its terminal signal to a detector, amplifier, and recorder. Recently an alternative method of measuring field distributions has been developed by Justice and Rumsey (5). A brief description of the method will be given, followed by the development of a modification which simplifies the instrumentation and adjustments involved.

The scattering method uses a hybrid junction as shown in Fig. 2.4 with the collinear arms terminated in an antenna and a resistive load. The E and H arms of the junction are connected to the signal source and the receiver. If the impedance of the load is equal to that of the antenna, no power is transferred from the signal source to the receiver. In practice the antenna must be tuned until the isolation between signal source and receiver is about 100 db. A thin, linear conductor having a length of one-half wavelength or less is then introduced at a point in the field of the antenna. This dipole is supported by thin nylon strings which cause negligible disturbance to the field. A current is induced on the dipole proportional to

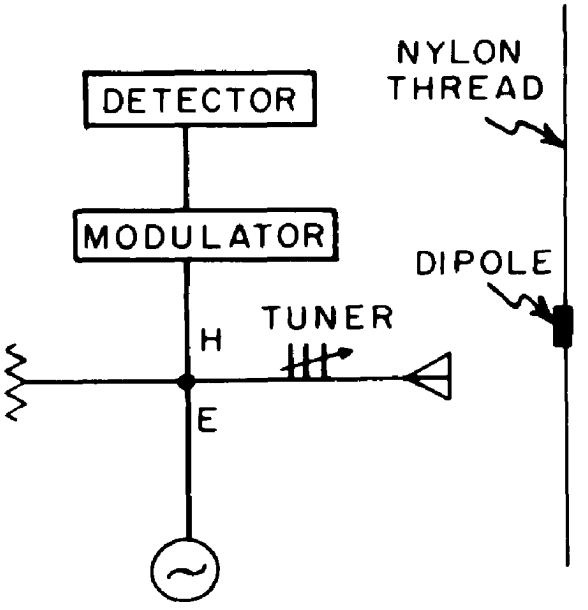

Plate IV

Fig. 2.4. Apparatus for electric field measurements with the scattering technique.

the component of the incident electric field parallel to its axis; that is, if the dipole is parallel to the z-axis, the current is proportional to E_z at that point in the absence of the dipole. Because of the current flowing on the dipole, a signal is radiated or scattered. This produces a reflected wave at the antenna input terminals as well as in other portions of space surrounding the scatterer. This reflected wave at the antenna terminals is separated by the hybrid junction and produces a voltage at the terminals of the receiver. It has been shown (5) that the voltage produced at the receiver terminals with the scatterer at a given position is proportional to the square of the tangential electric field intensity at the same position in the absence of the scatterer. Thus the amplitude and phase of the field at each point can be determined by measuring the phase

and amplitude of the received signal.

This scattering technique distorts the fields less than conventional probing methods since no cable is connected to the dipole. Fields in solid dielectric bodies can be measured with the scattering system by passing the dipole through a fine hole in the dielectric. However, the scatterer must be short to indicate the field at a point, and usually must be slender to discriminate against orthogonal polarization. Hence, the scattered signal is small. It will be shown that measurements with the scattering method are subject to errors from slight detuning of the hybrid junction and hence to frequency drift and temperature drift. Since the hybrid junction tuning is frequency sensitive, a monochromatic signal source is required. For this reason the source shown in Fig. 2.4 is operated unmodulated to avoid frequency modulation which generally occurs when a klystron is amplitude modulated. Care must be taken to prevent motion of any bodies (other than the dipole) in the antenna field during measurements.

To overcome these difficulties, a method will be described for amplitude-modulating the scattered wave. This will make it possible to relax the tuning and stability requirements and at the same time to increase the sensitivity of the measurements.

2. A MODULATED DIPOLE SCATTERER

The scattering from a dipole can be amplitude-modulated in several ways. The most practical method appears to be to place a nonlinear impedance in series with the dipole at its center, and to

modulate the impedance electronically. A Transitron type T7G subminiature germanium diode was somewhat arbitrarily selected as a nonlinear impedance. Cotton thread, made slightly conducting with a trace of Aquadag, was used not only to support the diode scatterer but also to connect an audio modulating voltage to it as shown in Fig. 2.5. Any field distortion due to the presence of the thread should be negligible because of its high resistance (500,000 ohms per ft) and small diameter (0.02 inch) even if the thread is parallel to the electric field vector, which is the worst case. In measurements of linearly polarized antennas the thread is aligned perpendicular to the electric field to minimize the rf currents on the thread and hence scattering by the thread.

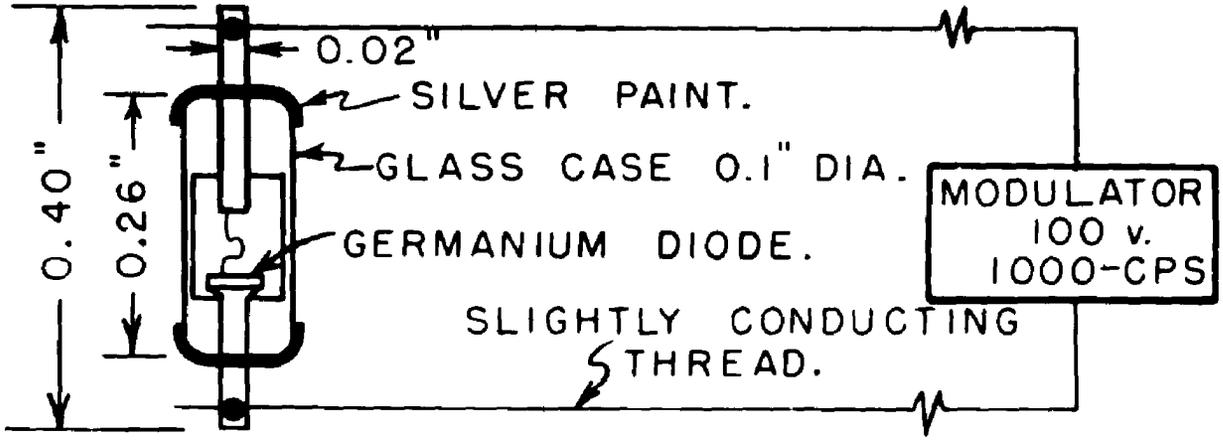

Plate I

Fig. 2.5. Modulated diode scatterer.

The dipole was resonated to the operating frequency of 9400 mc by applying silver paint over a small area of each end of the glass case of the diode as in Fig. 2.5. This resulted in a substantial

increase in the strength of the scattered field of the diode. The system shown in Fig. 2.5 was found to produce a scattered wave which was nearly 100 per cent modulated.

In the usual scattering system the dipole should have a length-to-diameter ratio of at least 30 to satisfy polarization requirements (5). However, this requirement can be relaxed considerably with a modulated dipole since the diode at the center will modulate only the axial component of current flowing on the dipole. Any circumferential component of current will be unmodulated and hence will produce no depolarization, as will be shown. By rotating the antenna and observing the signal level in the receiving arm of the hybrid junction, it was found that the modulated scatterer discriminated between orthogonal linear polarizations by at least 32 db. Of course, when modulation is applied to the scatterer, no modulation is introduced at any other point in the system.

3. ERROR ANALYSIS

To analyze certain errors involved in the usual scattering system shown in Fig. 2.4, let E_s denote the signal arriving at the detector by way of scattering from the dipole. If E_z is the electric field intensity component tangential to the dipole,

$$E_s \propto E_z^2. \tag{2.11}$$

There will also be an undesired signal E_u arriving at the detector even in the absence of the dipole, since the hybrid junction is never perfectly balanced.

Now, in the usual scattering method both the desired and undesired signals are modulated, and the resultant signal E arriving at the detector is

$$E = [\, E_s \cos \omega t + E_u \cos(\omega t + \beta)\,]\, m(t), \qquad (2.12)$$

where m(t) denotes the modulation function which may be taken to be the square wave shown in Fig. 2.6, ω is the microwave angular fre-

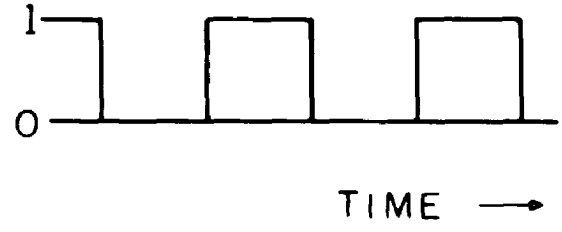

Plate VI

Fig. 2.6. Assumed modulation function m(t).

quency, and β is the phase angle of signal E_u. The error caused by E_u is maximum when β is zero or π, in which cases the detector indicates amplitudes

$$|E| = E_s \pm E_u. \qquad (2.13)$$

Thus, if the unbalance signal E_u is 20 db smaller than E_s, the measurement of E_s will have a possible error of $\pm$ 10 per cent. The measurement of the electric field distribution E_z may be in error by as much as $\pm$ 5 per cent.

It will now be shown that errors from unbalance signals can be eliminated if a modulated scatterer is employed. In order to accomplish this and at the same time increase the sensitivity of the measurements, it is assumed that a coherent detector such as shown

in Fig. 2.7 will be used. Modulation will be introduced at no point in the system other than at the dipole.

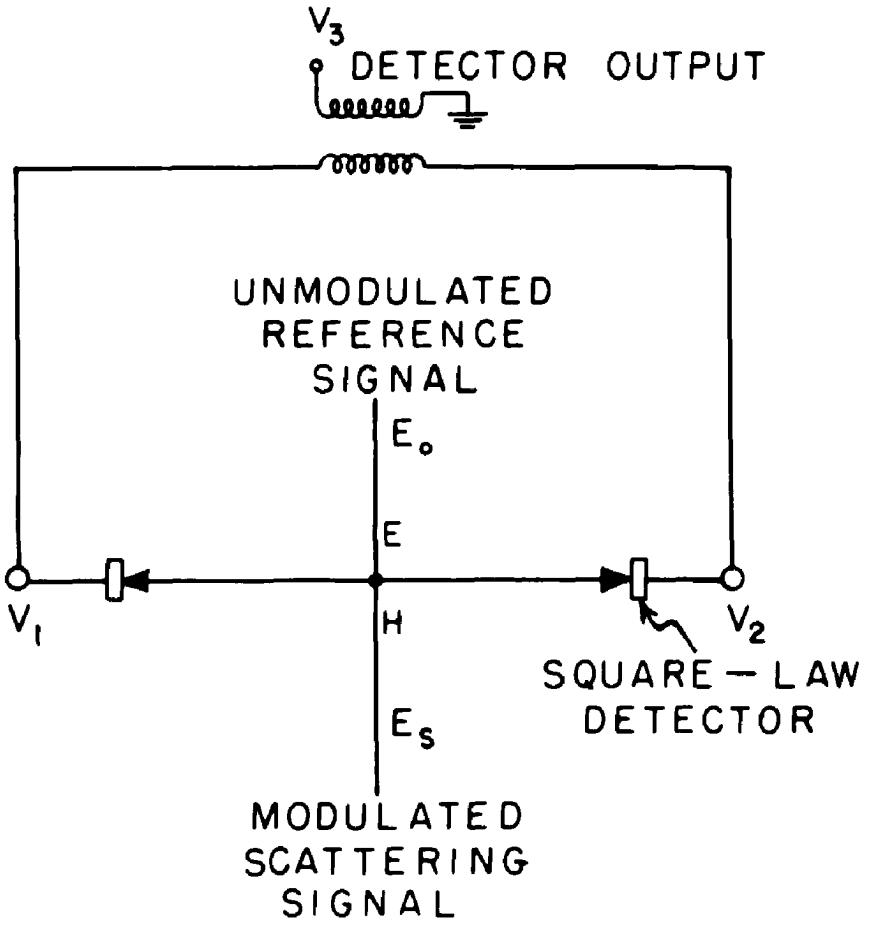

Plate XII

Fig. 2.7. Simplified diagram of coherent detector.

An unmodulated signal E_o direct from the microwave signal source is delivered to the E-arm of a hybrid junction. The modulated scattering signal E_s is applied to the H-arm. Some unmodulated unbalance signal E_u will undoubtedly accompany the scattered signal. Each of the two collinear arms of the hybrid junction is terminated with a square-law detector. The resultant signals E_1 and E_2 arriving at detectors 1 and 2 are

$$E_1 = E_o \cos \omega t + E_u \cos(\omega t+\beta) + E_s \cos(\omega t+\alpha)\, m(t), \qquad (2.14a)$$

and $$E_2 = E_o \cos \omega t - E_u \cos(\omega t+\beta) - E_s \cos(\omega t+\alpha)\, m(t). \qquad (2.14b)$$

The minus signs occur because of the properties of the hybrid junction. The power P_1 arriving at detector 1 is proportional to E_1^2. The only modulated components of this power are given by

$$P_1 = [\, E_s^2 \cos^2(\omega t+\alpha) + 2E_o E_s \cos \omega t \cos(\omega t+\alpha) + 2E_u E_s \cos(\omega t+\beta) \cos(\omega t+\alpha)\,]\, m(t). \qquad (2.15)$$

The audio response V_1 of detector 1 is found by averaging P_1 over one rf cycle:

$$V_1 = \frac{1}{2} E_s^2 + E_o E_s \cos \alpha + E_u E_s \cos(\alpha-\beta). \qquad (2.16a)$$

Similarly,

$$V_2 = \frac{1}{2} E_s^2 - E_o E_s \cos \alpha + E_u E_s \cos(\alpha-\beta). \qquad (2.16b)$$

The coherent detector response V_3 is obtained by subtracting V_2 from V_1 as is done by the audio transformer in Fig. 2.7, yielding

$$V_3 = 2\, E_o E_s \cos \alpha. \qquad (2.17)$$

Thus, the coherent detector response is independent of the phase or amplitude of any unbalance signal. In contrast with the usual scattering technique, theory indicates that the modulated scatterer method is immune to errors from unbalance signals.

If the phase of signal E_o is now shifted by 90°, one obtains

$$V_3 = 2\, E_o E_s \sin \alpha. \qquad (2.18)$$

Thus, it is possible to measure the real and imaginary components of the scattered signal E_s. The coherent detector also makes it convenient to plot phase distributions automatically (6).

Of course, coherent detection can be used with the usual type of scattering technique, but in this case it will not reduce the errors because the scattered signal and the unbalance signal are both modulated and cannot be distinguished.

4. EXPERIMENTAL RESULTS

It was desired to verify experimentally this predicted immunity of the modulated scattering system to errors from unbalance signals. A system similar to Fig. 2.4 was used with the modulated dipole of Fig. 2.5 and the coherent detector of Fig. 2.7. The electric field distribution was measured with the scattering method along a path near the aperture of a horn antenna. The measurement was repeated with various controlled amounts of unmodulated signal mixed in with the scattered signal where it was delivered to the detector. No error was detectable until the unmodulated signal E_u was increased to 15 db above the maximum scattered signal E_s, or 35 db above the minimum scattered signal for which accurate comparisons were made. Since in the usual scattering technique the unbalance signal must be 20 db below the smallest scattered signal to be measured accurately, it may be stated that the use of a modulated scattering system decreases the required hybrid junction isolation by 55 db. In the above experiment the detecting elements were type 1N23 crystals and the frequency was 9400 mc. Even more improvement might be expected using bolometers, since the immunity to unbalance errors depends on the use of square-law detecting elements. The performance also

depends on equalizing the gain of the two detecting elements in the coherent detector before subtraction takes place in the audio transformer. More accurate equalization than was used in the above experiment could readily be arranged.

Electric field distributions measured with the modulated diode were compared with measurements made with an ordinary dipole of the same length, using the probing path shown in Fig. 2.8 without the dielectric sheets. No detectable differences appeared in the two patterns. From these measurements and data on modulated diodes in waveguides, it is evident that the echo area of a modulated diode is constant for all reasonable levels of rf power. That is, no errors should arise from the nonlinear properties of the diode, at least for rf signal levels below 10 mw delivered to the diode.

C. PROBES FOR MICROWAVE NEAR-FIELD MEASUREMENTS

1. INTRODUCTION

Although the modulated scattering technique described in Section B has been found to be well suited for the measurement of fields near radomes, it is somewhat more complicated than direct probing methods. Therefore, direct probing may be preferred in some cases where it is adequate. For this reason, an empirical comparison of scatterers and probes of various sizes was made and will be described after a few general comments on probes.

A probe for accurately measuring the field intensity distribution near a radio-frequency source must meet the following requirements:

a. Any distortion of the fields by the probe and its cable must not seriously affect the accuracy of the measurements.

b. The aperture of the probe must be small enough to measure essentially the field at a point.

c. The probe must have the desired polarization to within sufficient accuracy.

d. The probe must deliver a signal voltage large enough to permit accurate measurement.

The aperture size requirement on probes has been analyzed by Woonton (7) who concluded that a probe should be no longer than one-half wavelength and no more directive than a half-wave dipole.

It is apparent that the performance of any given probe may depend on the environment in which it is placed. Also, the design of a probe may be simplified if one has a knowledge of certain characteristics of the fields to be measured. For example, if the fields are known to have a slow spatial variation, the probe aperture size can be increased. If the polarization of the field is known, the polarization requirements on the probe can often be relaxed. A smaller probe may be feasible if the transmitter power or receiver sensitivity can be increased. In short, it is more realistic to select the probe which is most satisfactory for the particular type of measurements of interest than to seek a universal probe to be used in all situations.

Dipole probes are perhaps the most popular type for near-field measurements. The dipole is generally connected to a coaxial line

through a balun. The dipole and balun must be carefully designed and constructed to obtain satisfactory results. Small horns or open-ended waveguides may also be used as probes. These require no balun and are quite simple to construct.

2. MEASUREMENTS

To determine the accuracy of a probe it would be desirable to use the probe to measure a known field. Any errors in the measurements would then be immediately apparent. However, it is not a simple matter to set up a suitable known field. Known fields can be set up in waveguides and might provide a suitable test of the accuracy of scatterers. The waveguide test would very likely prove to be too severe for many probes, and it is felt that a probe should be tested in a situation similar to that in which it is intended to be used.

Very few antenna fields are rigorously known. A good physical model of the infinitesimal dipole, the fields of which are well known, might be obtained by inserting a short, thin stub through a hole in a large conducting ground plane. This might provide a standard field for testing probes, and would be an interesting project. However, even in this case the accuracy would be limited by such factors as the finite size of the ground plane. Furthermore, a probe which gives sufficiently accurate measurements of these simple fields might prove to be inadequate for measuring the complicated fields near a radome.

Therefore, to investigate the near-field measurement problem, a field was set up which was typical of the fields near a radome.

This was accomplished by placing a wedge-shaped dielectric shell in front of a horn antenna and choosing a straight line probing path parallel to the horn aperture as indicated in Fig. 2.8. The horn was connected to a type X-13 Varian klystron tuned to 9375 mc, corresponding to a wavelength of 1.26 inches. The field distribution was recorded by automatic phase (6) and amplitude plotters as the probe was moved along the probing path by a motor. The phase measurements were made with a balanced coherent detector using type 1N23 crystals. A Sperry type 821 bolometer was used as a square-law detector for the amplitude measurements.

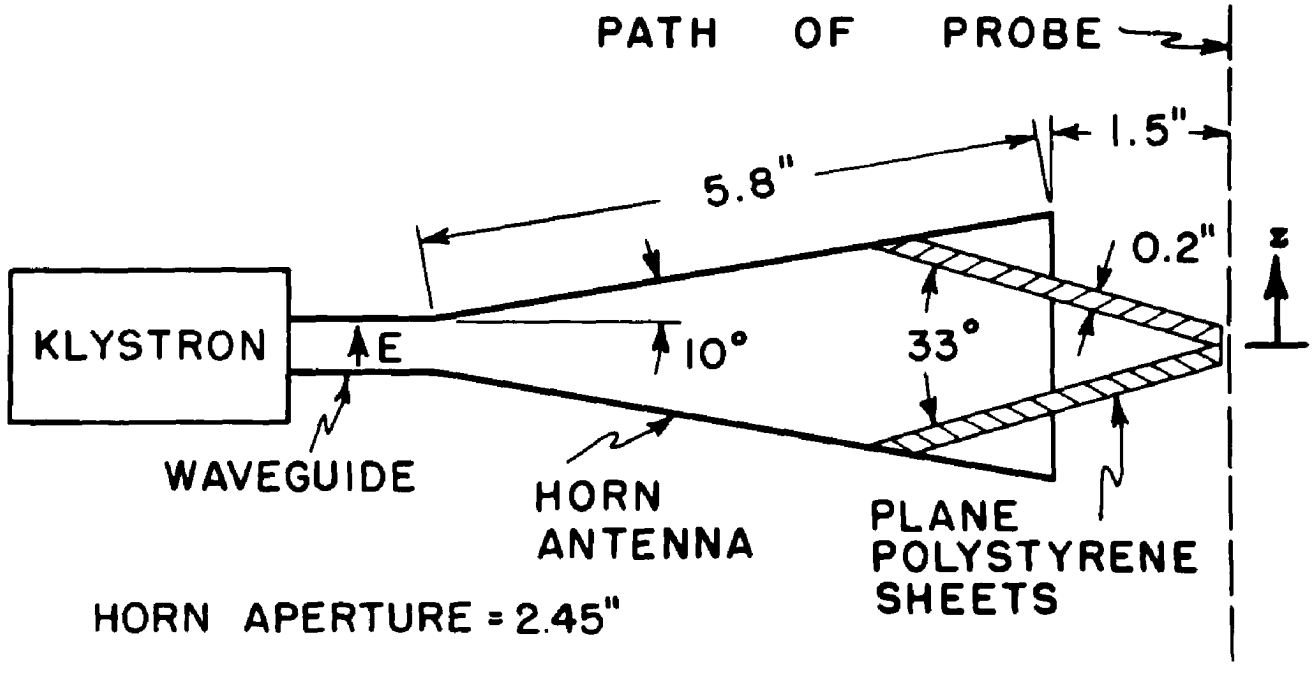

Plate XIII

Fig. 2.8. Experimental arrangement for investigating probes.

These measurements were repeated using several types of probes, including a small horn and three sizes of open-ended waveguide. The orientation of a probe with its waveguide feed is indicated in Fig. 2.9.

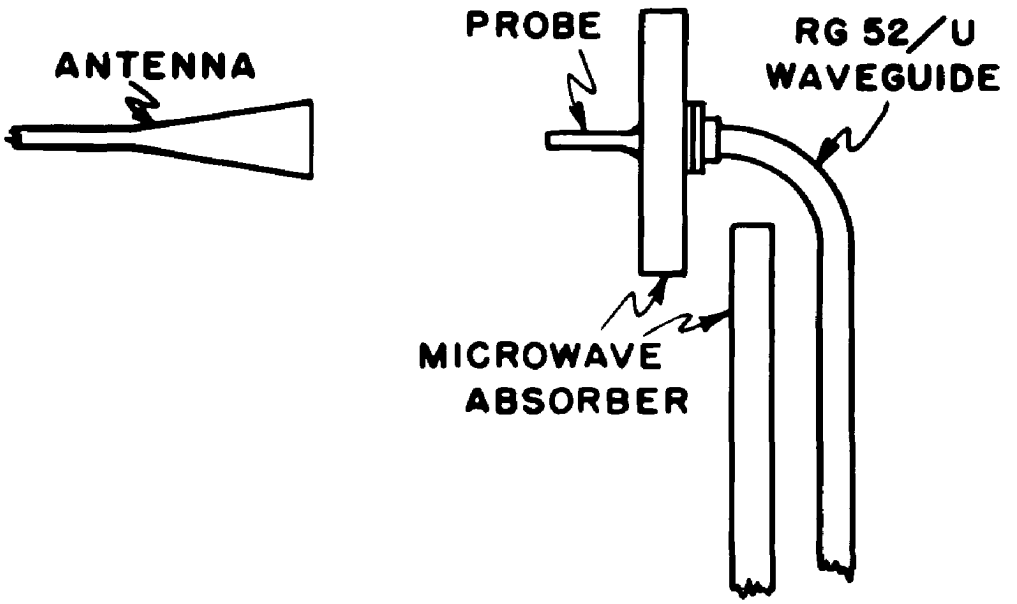

Plate IX

Fig. 2.9. Orientation of probe 4 and waveguide feed.

Waveguide transition sections, tapered in both dimensions, were used to couple the two smallest probes to standard X-band waveguide as shown in Fig. 2.10. The outside surfaces of the probes were covered

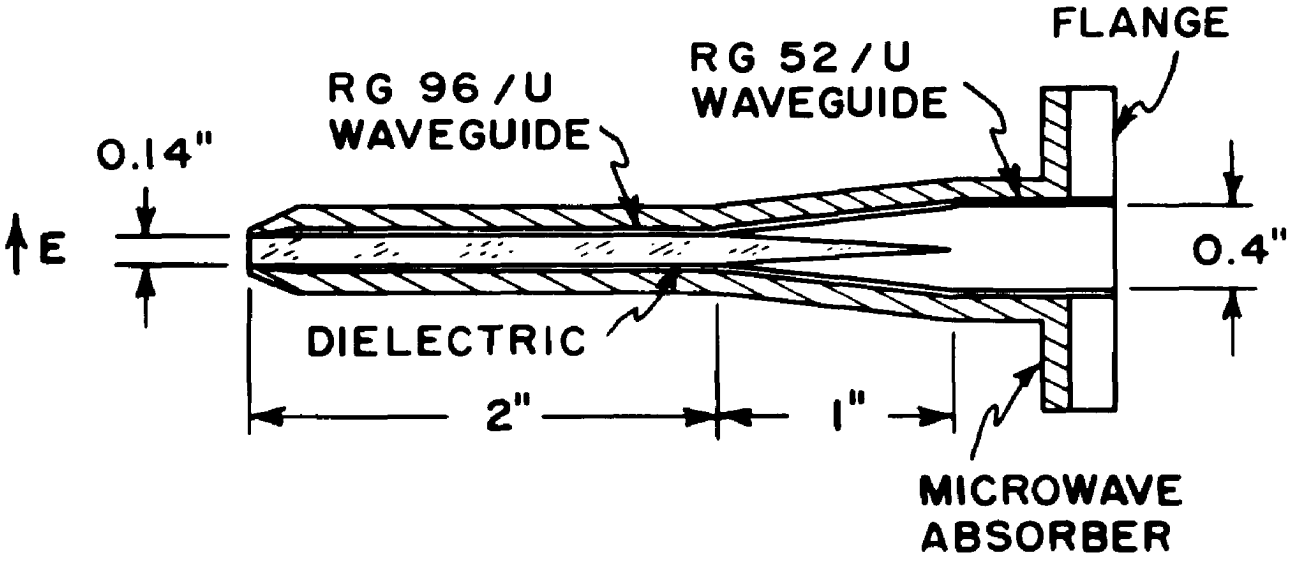

Fig. 2.10. Cross section of probe 4 showing waveguide transition.

Plate X

with microwave absorber to reduce distortion of the fields. It was necessary to fill the smaller waveguide probes with dielectric materials to permit transmission of energy through them at 9375 mc. Pertinent information on each probe is listed in Table II.

TABLE II

Probes Which Were Compared

Probe Number	Description	Aperture size (inches) E-plane	H-plane	Dielectric Constant
1	horn	1.13	0.90	1
2	open-ended waveguide	0.40	0.90	1
3	"	0.18	0.42	4
4	"	0.14	0.28	11

The measurements were repeated with the scattering technique, using scatterers of two different lengths. The dimensions of the scatterers are listed in Table III.

TABLE III

Scatterers Which Were Compared

Scatterer Number	Length (inches)	Diameter (inches)
1	0.5	0.005
2	0.3	0.050

It will be noted that a larger diameter of wire was used for the shorter scatterer. This was necessary in order to obtain a signal large enough to record accurately, since the modulated scattering

method had not yet been developed. As the polarization of the field was essentially linear and the scatterer was oriented almost parallel with the electric field intensity vector, no loss of accuracy was anticipated due to the increased diameter. Useful measurements could not be made with scatterers less than 0.3 inch long with the equipment in use, although the length could be reduced if the transmitter power or receiver sensitivity were increased.

Fig. 2.11 shows the field distribution as measured by the scattering method. It is noted that the shorter scatterer gave the

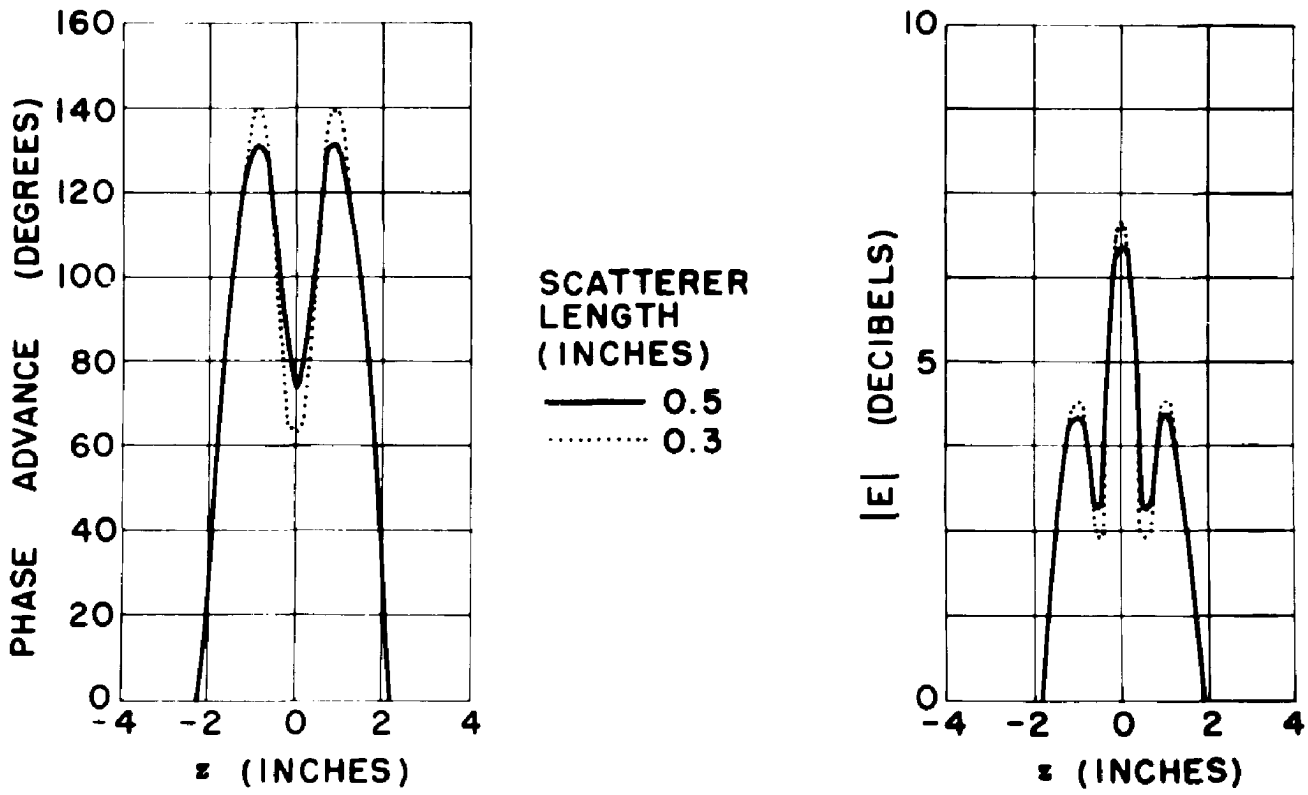

Plate XI

Fig. 2.11. Relative phase and amplitude distributions as measured with scatterers.

higher peaks and deeper nulls. Presumably the shorter scatterer is the more accurate one, and hence the results obtained with it are

replotted in Fig. 2.12 for comparison with the probes.

The averaging effect which takes place in the aperture of probe 1 (the small horn) is obvious in both the amplitude and phase patterns of Fig. 2.12. Otherwise, the phase patterns are in good agreement. The amplitude patterns show quite strikingly the steady increase in resolution as the probe aperture dimensions are reduced. The shortest scatterer which could be used had an E-plane dimension twice that of the smallest probe. As a result, the scatterer reduced the peaks by 3 db and increased the level at the nulls by 2 db as compared with probe 4. Although probe 4 has a much smaller aperture than probe 3, these two probes yielded patterns which are in close agreement. It is therefore felt that no additional improvement in accuracy would be obtained by further reduction in the aperture size.

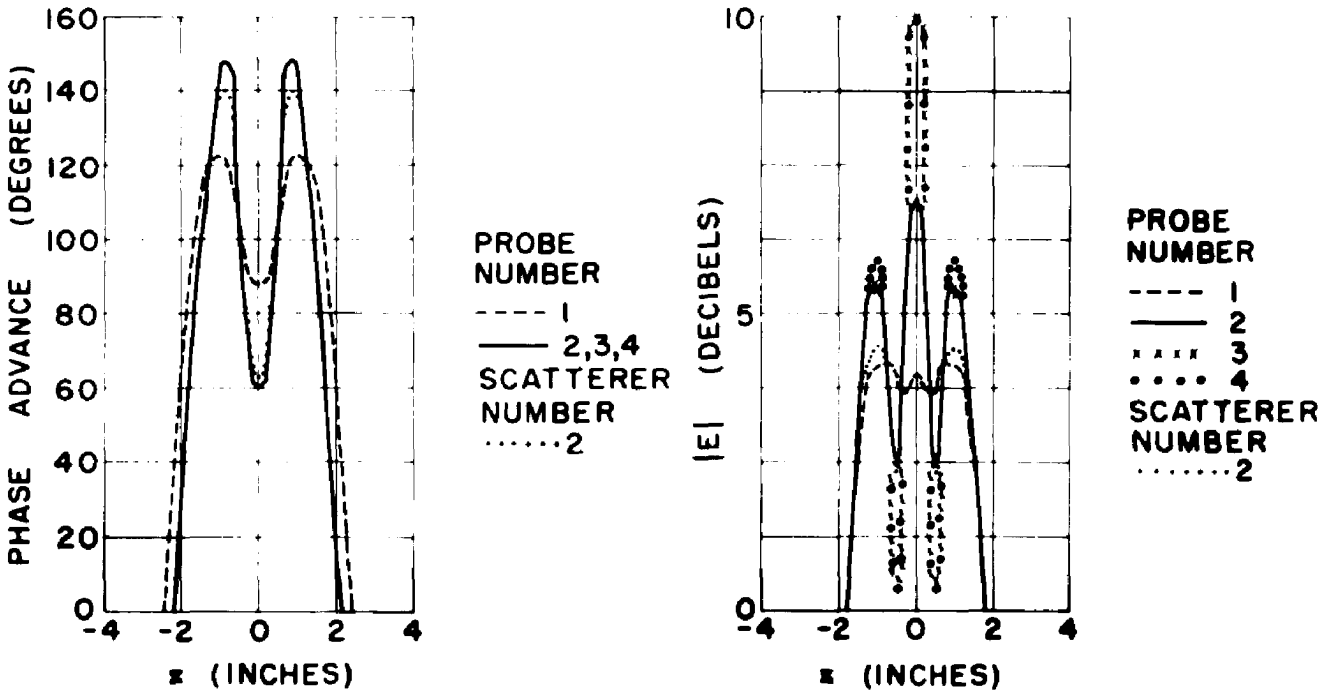

Plate XII

Fig. 2.12. Relative phase and amplitude distributions as measured with various probes and scatterer 2.

In order to further test the accuracy of probe 4, it was used to measure the fields on a path six inches from the aperture of the horn shown in Fig. 3.2. For convenience, the real and imaginary components of the field distribution were recorded using a coherent detector. The measured fields, shown in Fig. 3.3, were used to predict the H-plane far-field pattern of the horn. Good agreement was obtained with the measured far fields as is evident in Fig. 3.4. Equally good results were obtained in far-field calculations based on the fields measured on a path only 1.2 inches from the horn aperture with probe 4.

By using probe 4 to measure the field of a rotatable dipole it was found that the probe discriminated between cross linearly polarized waves by at least 38 db.

D. REFERENCES

1. M. E. Brodwin, C. M. Johnson, and W. M. Waters, "Low Level Synchronous Mixing", Convention Record of the I. R. E. 1953 National Convention, Part 10.

2. R. L. Cosgriff, "A Study of Detectors and Amplifiers Used in Antenna Instrumentation", Technical Report 487-5, Antenna Laboratory, The Ohio State University Research Foundation, December 28, 1953.

3. J. Bacon, "Selective Bolometer Amplifier", Technical Report 301-24, Antenna Laboratory, The Ohio State University Research Foundation, September 15, 1950.

4. R. G. Kouyoumjian, "The Calculation of the Echo Areas of Perfectly Conducting Objects by the Variational Method", Technical Report 444-13, Antenna Laboratory, The Ohio State University Research Foundation, November 15, 1953, pp. 29 and 80-84.

5. R. Justice and V. H. Rumsey, "Measurement of Electric Field Distributions", to appear in the Transactions of the I. R. E. Professional Group on Antennas and Propagation, October 1955.

6. J. Bacon, "An Automatic X-Band Phase Plotter", Proceedings of the National Electronics Conference, Chicago, Illinois, October 1954.

7. G. A. Woonton, "On the Measurement of Diffraction Fields", The Eaton Electronics Research Laboratory, McGill University, Montreal, Quebec, Symposium on Microwave Optics, vol. 2, June 1953.

III. SIMPLIFIED CALCULATION OF ANTENNA FAR-FIELD PATTERNS

1. INTRODUCTION

The analysis of far-field distortion produced by a radome is usually divided into two steps. First, the fields on a surface just outside the radome are calculated by using approximate methods of describing the transfer of energy from the antenna through the radome. Next, the fields on the reference surface are integrated to determine the far-field pattern. In this chapter, the surface integration involved in the far-field analysis is considered with the objective of simplifying the numerical computations. The results will be found applicable to similar integrals which arise in the formulation used in Chapter IV.

Given the electric and magnetic field intensity distributions E and H on some surface S enclosing a transmitting antenna, it is desired to determine the far-field pattern of the antenna. While the solution may be simple in principle, in practice the numerical computation is lengthy and may require the use of large computers. The antenna may be replaced by equivalent electric and magnetic currents J and K flowing on S, where

$$J = n \times H, \tag{3.1a}$$

and

$$K = E \times n, \tag{3.1b}$$

where n is a unit vector in the direction of the outward drawn normal to S. Two vector potentials A and F may be defined in the usual manner (1):

$$A = \mu \iint_S \frac{Je^{-jkr}}{4\pi r}\, ds, \tag{3.2a}$$

and

$$F = \varepsilon \iint_S \frac{Ke^{-jkr}}{4\pi r}\, ds, \tag{3.2b}$$

where k is the propagation constant, μ is the permeability, and ε is the dielectric constant of the homogeneous medium which is assumed to occupy all space outside of S, and r is the distance from a point on S to the observation point. The electric field intensity everywhere on the source-free side of S is given (1) by

$$E = -\frac{\nabla \times F}{\varepsilon} - j\frac{\nabla \times \nabla \times A}{\omega\mu\varepsilon}, \tag{3.3}$$

where ω is the angular frequency of the source.

The problem is simplified if S is chosen to be an infinite plane, in which case a knowledge of the tangential electric or magnetic field on the plane is sufficient to determine the fields in the half-space not including the source. This has been shown by Rumsey (2) by considering the radiation produced by J and K when S is lined with a perfect conductor. Image theory is applied to show that the fields will be just twice those produced by J or K alone radiating in free space. Thus, if S is a plane,

$$E = -2\frac{\nabla \times F}{\varepsilon} = -2j\frac{\nabla \times \nabla \times A}{\omega\mu\varepsilon}. \tag{3.4}$$

This result has been verified by the author by another approach which, however, is more lengthy and need not be presented here. Using the coordinate system shown in Fig. 3.1, the first part of eq. 3.4 yields the following E-plane and H-plane ($\phi = 0$ and $\theta = 90^\circ$ planes) far-field patterns associated with the z-polarized component

$E_z(y,z)$ of the near field:

$$E_\theta(\theta) = \iint E_z(y,z)e^{jkz\cos\theta}\,dy\,dz, \tag{3.5a}$$

and

$$E_\theta(\phi) = \cos\phi \iint E_z(y,z)e^{jky\sin\phi}\,dy\,dz. \tag{3.5b}$$

Since only the relative far-field patterns are of interest here, the constants of proportionality have been omitted in these expressions. This will also be done elsewhere in this chapter with no further comment.

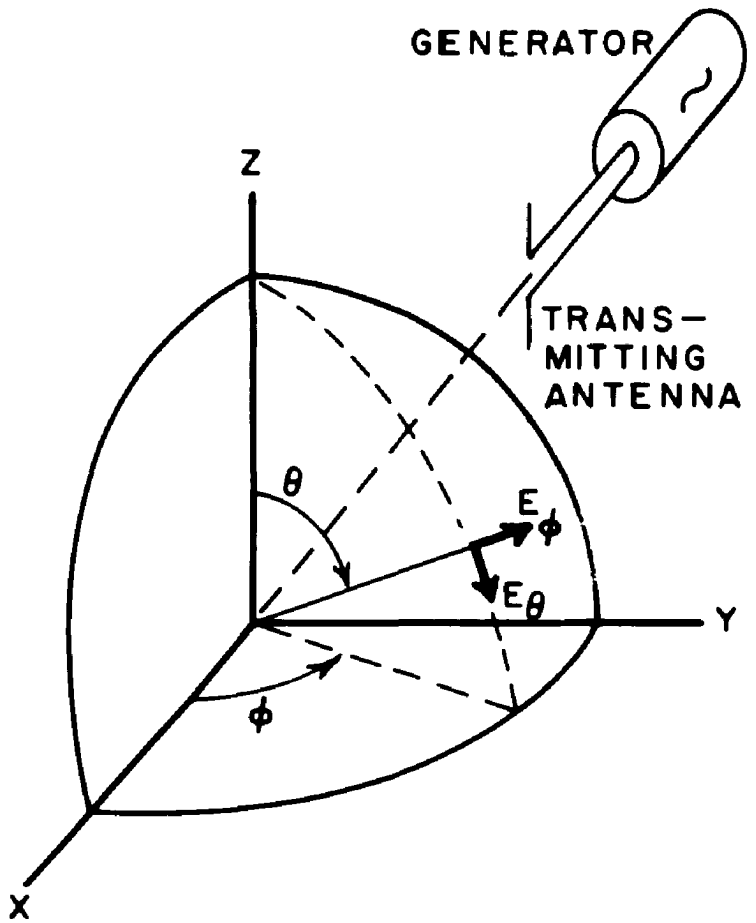

Plate XIII

Fig. 3.1. Coordinates used in far-field calculations.

Expressions similar to eqs. 3.5 give the patterns associated with a y-polarized near field. By superposition of the far fields

associated with these two near-field components, the resultant far-field pattern is obtained even for elliptically polarized antennas. Hence, it will be sufficient to consider only linearly polarized fields.

Equations 3.5 may be contrasted with the approximate expressions in common use for far-field calculations (3). The exact expressions (eqs. 3.5) are no more complicated than the approximate ones generally used. In certain cases the difference between the exact and approximate expressions is appreciable.

Unless $E_z(y,z)$ is a particularly simple function, the surface integrations in eqs. 3.5 are quite time consuming. A simplification can be achieved in certain practical cases where the near field is, to a good approximation, separable, i.e.,

$$E_z(y,z) = Y(y)\, Z(z). \tag{3.6}$$

In this event, eqs. 3.5 reduce to

$$E_\theta(\theta) = \int Z(z) e^{jkz\cos\theta}\, dz, \tag{3.7a}$$

and

$$E_\theta(\phi) = \cos\phi \int Y(y) e^{jky\sin\phi}\, dy. \tag{3.7b}$$

The separability assumption has been found to yield satisfactory results in the case of pyramidal horns and small paraboloid antennas. This is to be expected with horns, since it is well known (4) that the E-plane pattern of a horn is substantially independent of the aperture width in the H-plane, and vice versa.

A common method of evaluating the integrals in eqs. 3.7 is to approximate the fields Z(z) and Y(y) with simple functions for which the corresponding far fields are known. For example, Y(y) might be

approximated by the first few terms of its power series expansion or Fourier series expansion. However, a good approximation often requires several terms, and the procedure for finding the coefficients is lengthy. Even when this has been accomplished it still remains to superimpose the rather complicated far-field contributions corresponding to each term.

If the notation Y(y) is replaced with $E_z(y)$, eq. 3.7b can be written

$$E_\theta(\phi) = \left[\int E_z(y)\cos(ky\sin\phi)\, dy + j \int E_z(y) \sin(ky \sin\phi)\, dy \right] \cos\phi \qquad (3.8)$$

A systematic procedure for evaluating the first integral in eq. 3.8 will next be described. The method can immediately be applied to the second integral also, and hence to the integrals in eqs. 3.7.

2. SIMPLIFIED APPROXIMATE CALCULATIONS

As shown, integrals of the following form appear in the far-field expressions:

$$E_\theta(\phi) = \cos\phi \int E_z(y) \cos(ky \sin\phi)\, dy. \qquad (3.9)$$

Many antennas set up near fields which are symmetrical. In this case, eq. 3.9 gives the H-plane far-field pattern. If α denotes the phase of $E_z(y)$, the near field can be resolved into real and imaginary components as follows:

$$E_z(y) = |E_z| (\cos\alpha + j \sin\alpha) = R(E_z) + j\, I(E_z). \qquad (3.10)$$

Now the complex integral in eq. 3.9 can be resolved into two real integrals and can be approximated by the real summations:

$$E_\theta(\phi) \approx \cos\phi \sum_{m=1,3,5\cdots}^{n} \{ R[E_z(my_o)] + jI[E_z(my_o)] \} \cos(kmy_o \sin\phi). \quad (3.11)$$

Any desired degree of approximation can be obtained by choosing y_o small enough; however, the labor increases as y_o is decreased. If the value chosen for y_o is greater than about 0.1 wavelength, a better approximation to eq. 3.9 is given by

$$E_\theta(\phi) \approx \sum_{m=1,3,5\cdots}^{n} \{ \underline{R}[E_z(my_o)] + j\,\underline{I}[E_z(my_o)] \} A_m(\phi), \quad (3.12)$$

where $\underline{R}$ and $\underline{I}$ denote the average values of the real and imaginary components over the interval $(m-1)y_o < y < (m+1)y_o$, and

$$A_m(\phi) = \cos\phi \int_{(m-1)y_o}^{(m+1)y_o} \cos(ky \sin\phi)\, dy. \quad (3.13)$$

If eq. 3.12 is used, the continuous near-field distribution $E_z(y)$ is in effect approximated by an array of uniformly excited line sources, each of length $2y_o$ and of the proper strength. The relative far-field patterns of these line sources are the $A_m(\phi)$, and eq. 3.12 superimposes the individual far-field contributions in their proper strengths. The summation must be extended along the y-axis to a point where the field amplitude becomes and remains negligible. Satisfactory results have been obtained by carrying the summation out to a point where E_z becomes less than 1 per cent of its maximum amplitude.

The far-field calculation method was tested at 9400 mc on the horn antenna shown in Fig. 3.2. The near field was measured with the

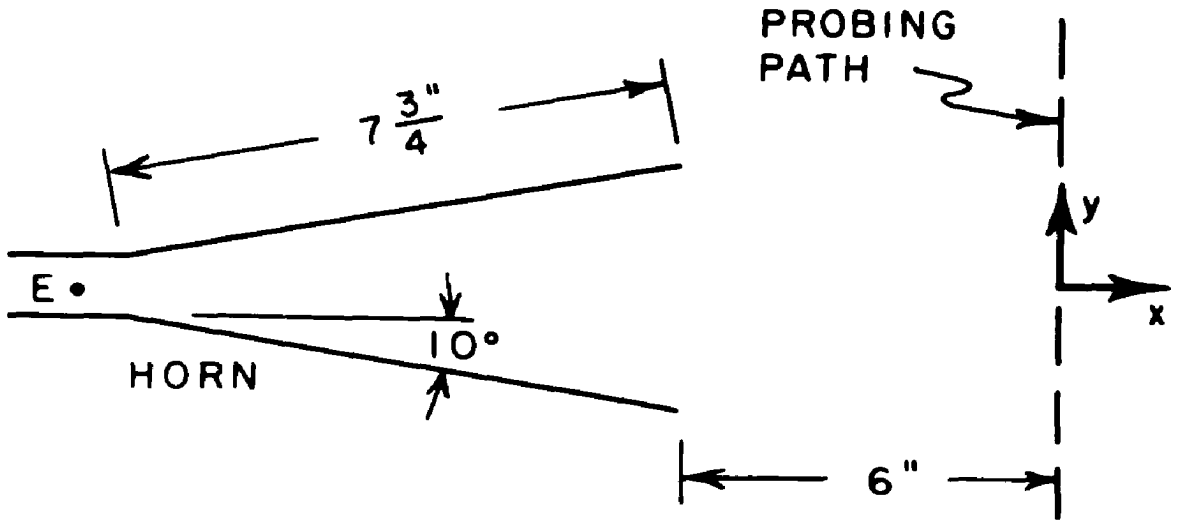

Plate XIV

Fig. 3.2. Pyramidal horn antenna used to test the far-field calculation method.

small open-ended waveguide probe (probe 4) described in Chapter II. The probing path was a straight line 6 inches from the horn aperture. For convenience in performing the calculations, the real and imaginary components of E_z were measured directly rather than the amplitude and phase. This was accomplished by using the balanced coherent detector described in Chapter II. The measured fields are reproduced in Fig. 3.3. Using the measured near fields, the H-plane far-field pattern of the horn was calculated from eq. 3.11 with y_o = 0.1 inch and from eq. 3.12 with y_o = 0.25 inch and 0.5 inch. The measured pattern and the three calculated patterns are compared in Fig. 3.4. The measurements and calculations were carried out only through the main lobe of the far-field pattern since only this region was of interest in the radome problem being considered.

Of course, the largest value of y_o which will give accurate far-field calculations depends on the nature of the particular near-fields

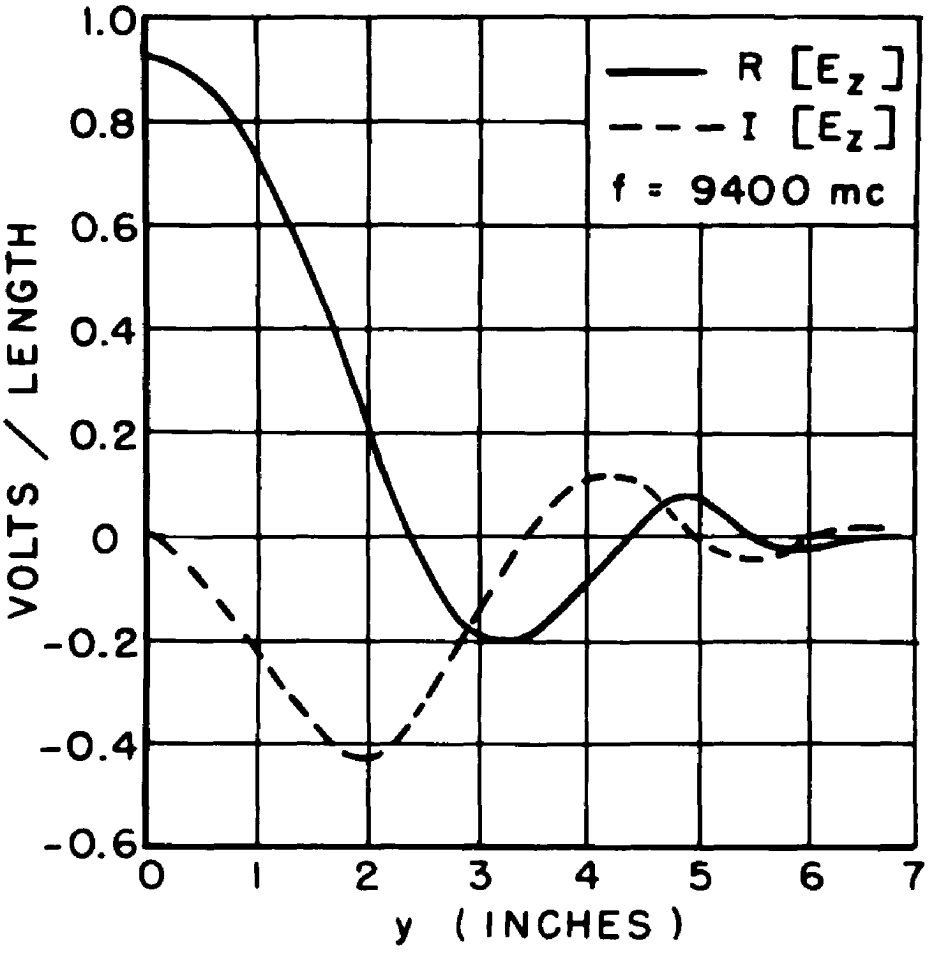

Plate XV

Fig. 3.3. Fields of horn shown in Fig. 3.2.

involved. It may be practical to use a larger value of y_o when working with fields which vary more slowly with y. In the example shown in Fig. 3.4, when y_o is reduced to 0.1 inch (about 0.08 wavelengths) the error arising from replacement of the integral in eq. 3.9 with the summation in eq. 3.11 diminishes to the same order of magnitude as the experimental errors involved in measuring the near and far fields.

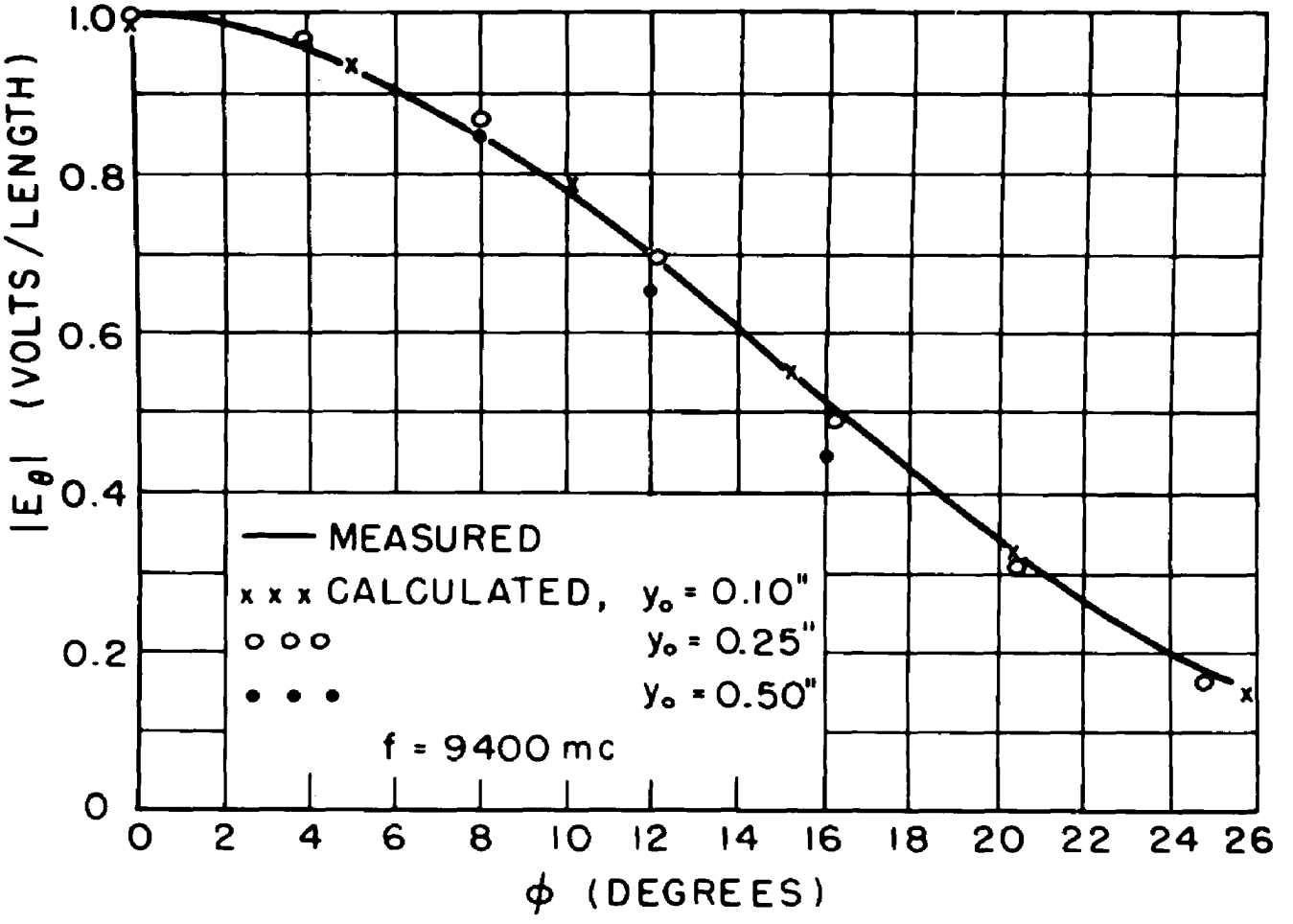

Plate XVI

Fig. 3.4. Measured and calculated H-plane far-field patterns of horn shown in Fig. 3.2.

3. EXAMPLES

To indicate the usefulness and accuracy of the simplified calculations, several examples are presented. Figure 3.5 shows the measured and calculated E-plane far-field patterns of the horn of Fig. 3.2. The calculations were based on the near fields $E_z(z)$ measured on a line 6 inches from the horn aperture. A formula similar to eq. 3.11 was derived from eq. 3.7a and was used for the E-plane calculations.

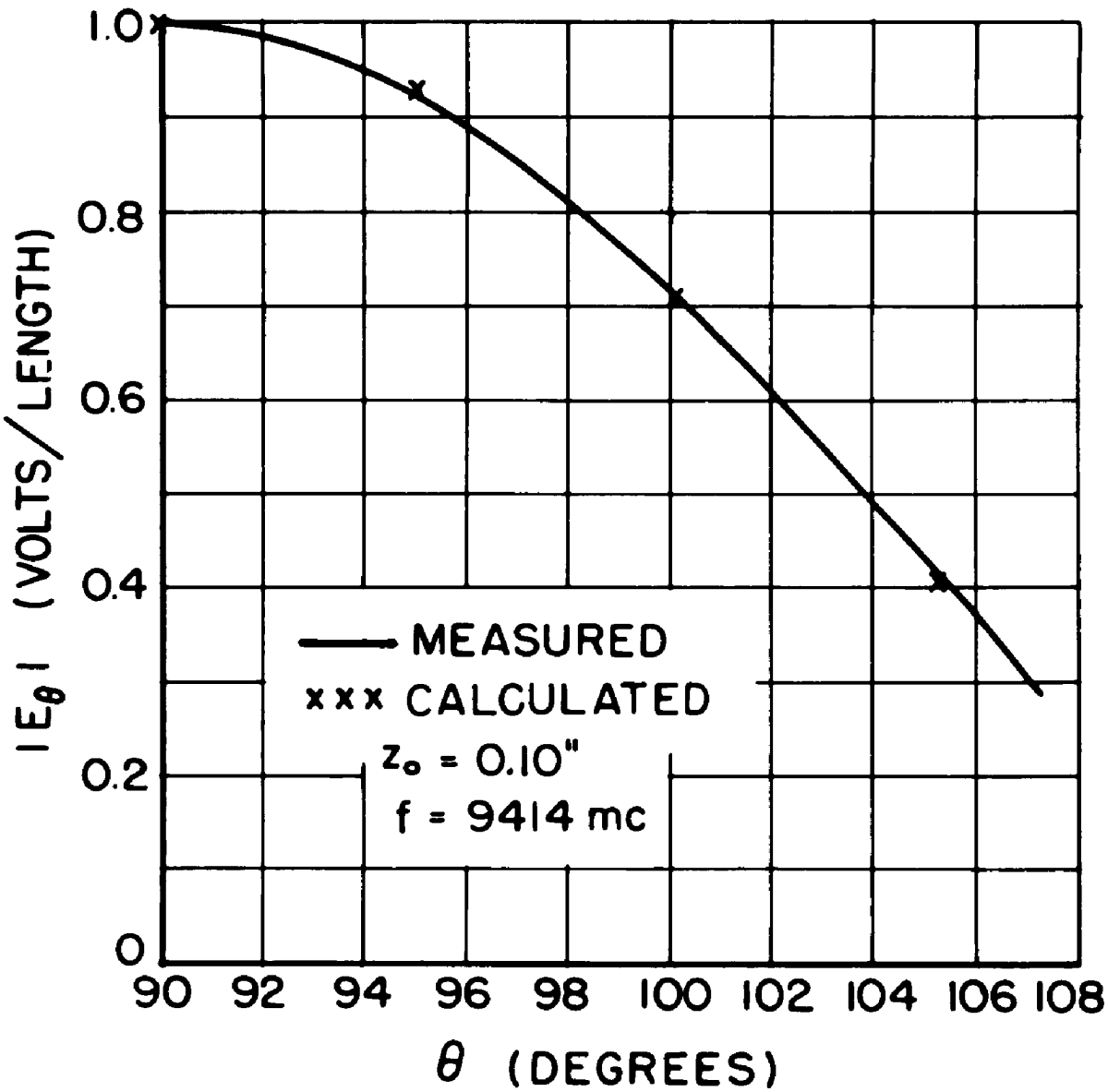

Plate XVII

Fig. 3.5. E-plane far-field pattern of horn shown in Fig. 3.2.

Equation 3.12 was used to calculate the H-plane far-field pattern of the small paraboloid antenna shown in Fig. 3.6. The measured and calculated patterns are shown in Fig. 3.7.

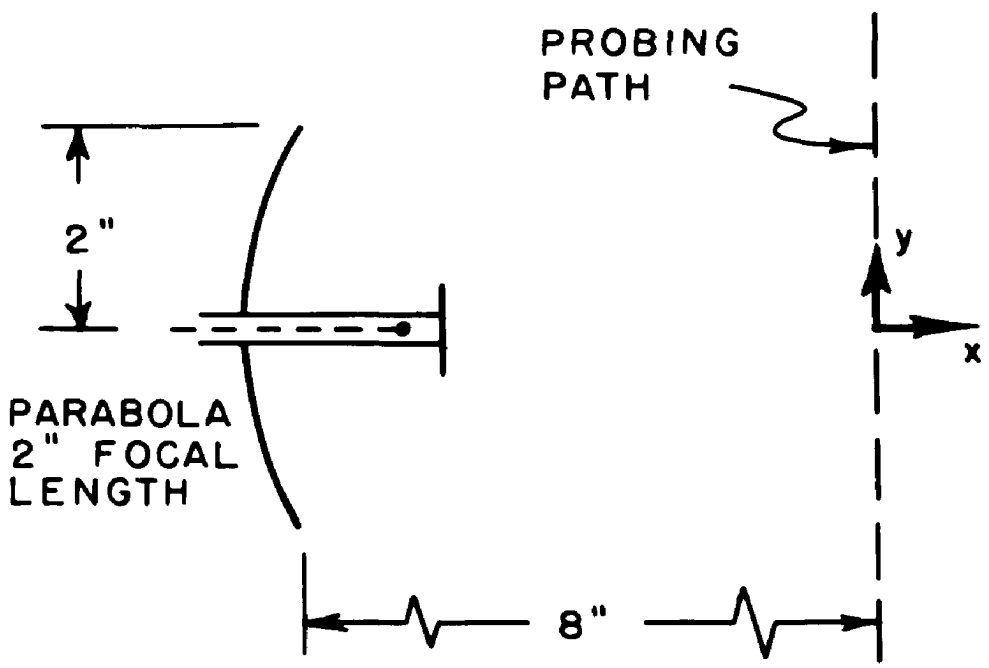

Plate XVIII

Fig. 3.6. Paraboloid antenna used to test the far-field calculations.

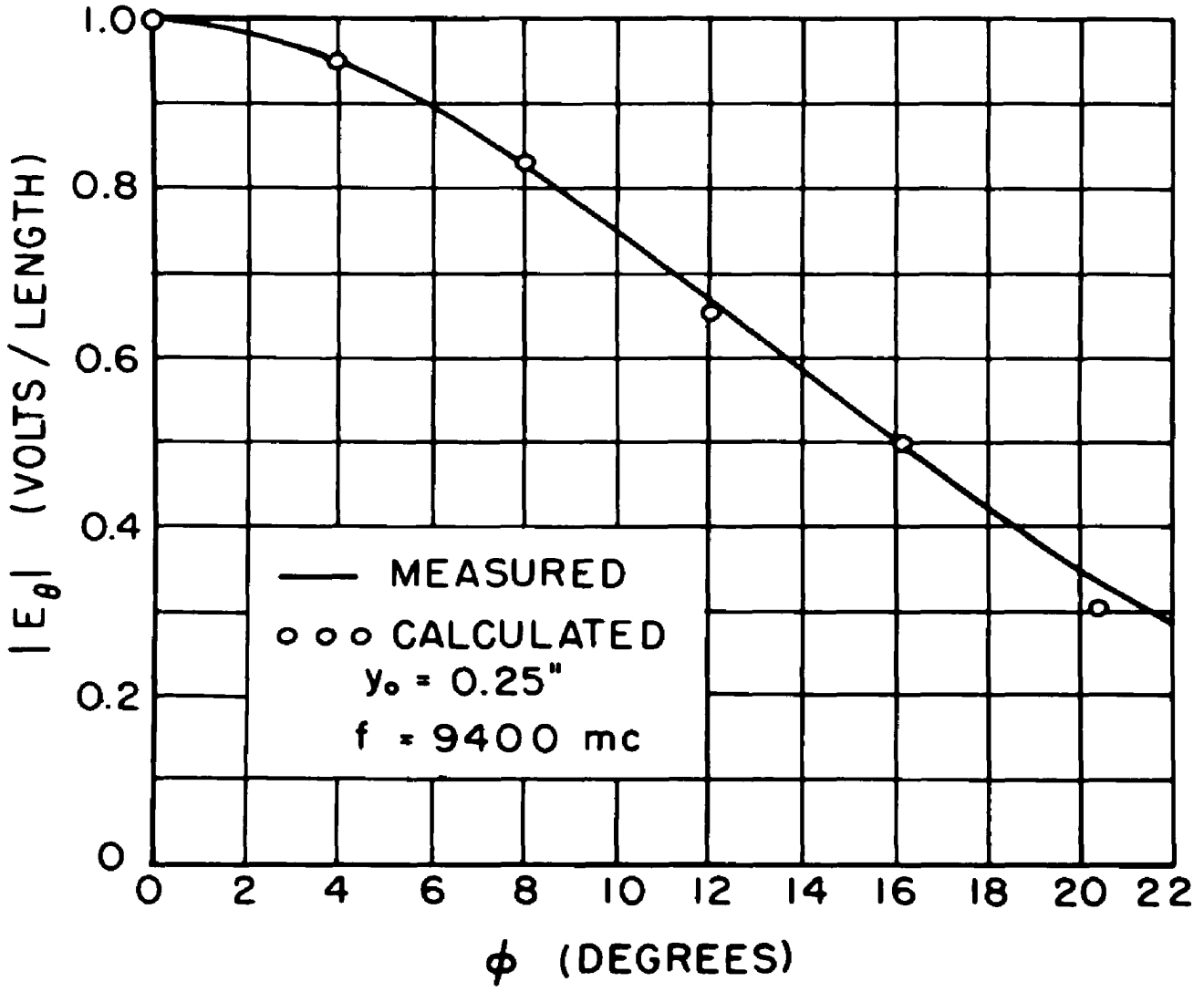

Plate XIX

Fig. 3.7. H-plane far-field pattern of paraboloid shown in Fig. 3.6.

Finally, a hollow dielectric wedge was placed over the horn as shown in Fig. 3.8. The measured and calculated (eq. 3.12) far fields are shown in Fig. 3.9. The far-field pattern of the horn alone is also shown for comparison.

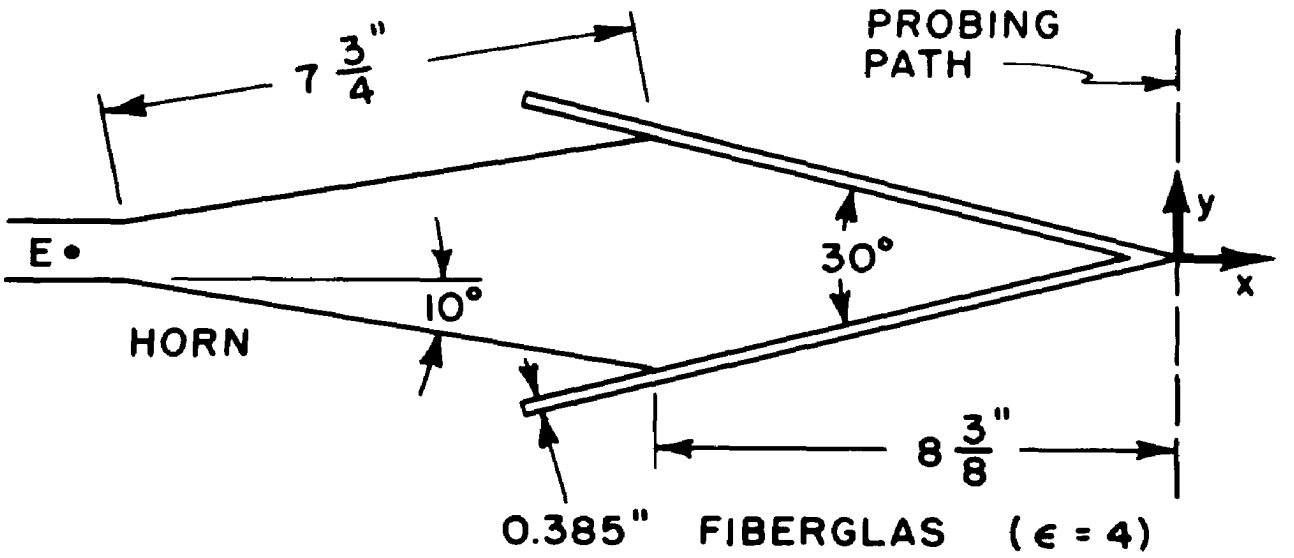

Plate XX

Fig. 3.8. Horn with hollow dielectric wedge used to test the far-field calculations.

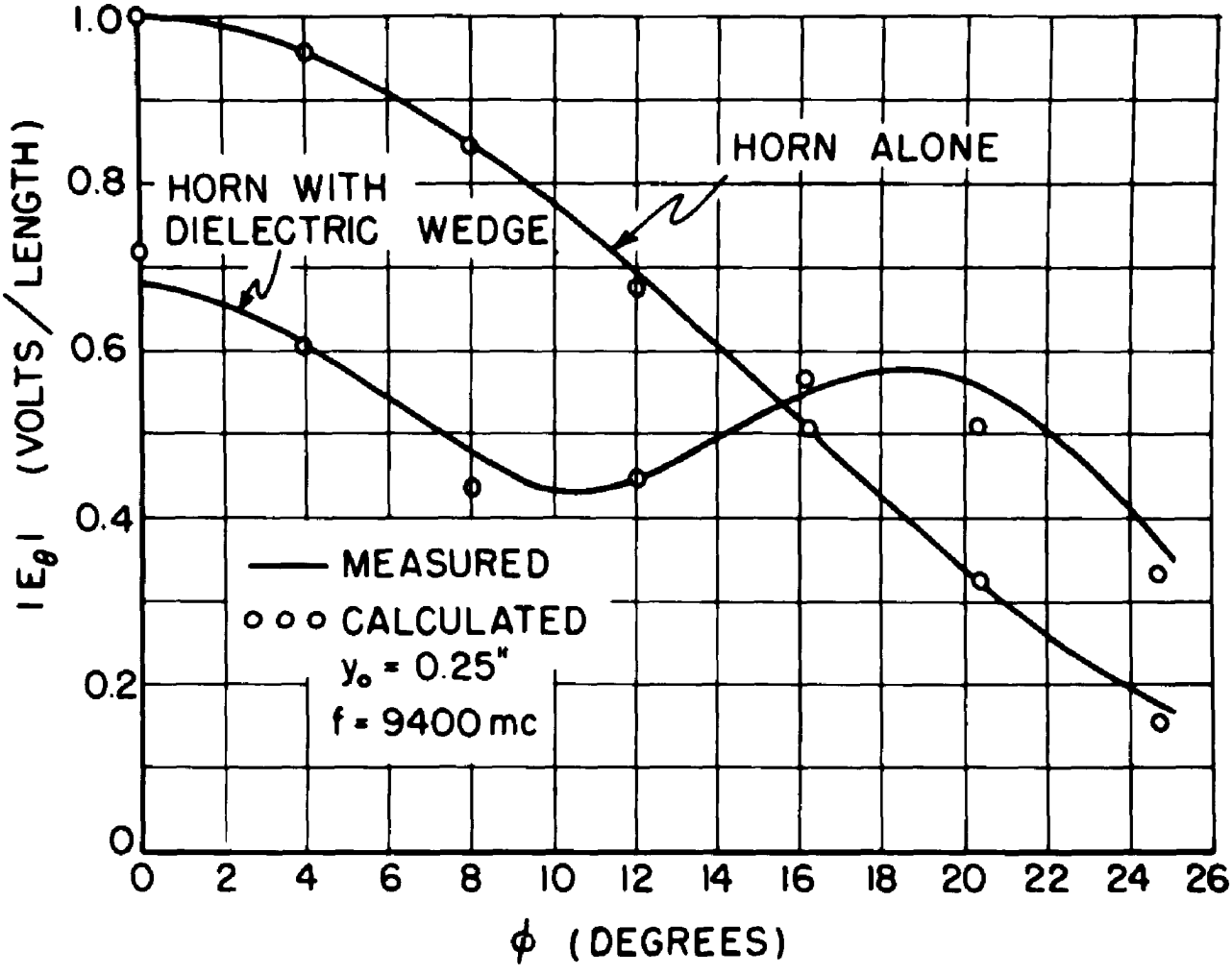

Plate XXI

Fig. 3.9. H-plane far-field patterns of horn with and without wedge.

4. USE OF AN INCLINED REFERENCE PLANE

In Chapter IV it will be found desirable to make far-field calculations based on near fields which are given on an infinite plane surface inclined at some angle from the antenna aperture. This problem arises in the analysis of transmission through a plane dielectric sheet. It is also encountered in radome analysis when the fields on the radome surface have been calculated and it is

desired to use these fields to determine the far-field pattern. It is customary to first project the radome surface fields to a plane surface parallel with the antenna aperture. While this simplifies the calculations, it introduces a source of error since an approximate method of projection is usually employed. Straight lines, parallel with the antenna axis, are drawn from each point on the radome surface to the reference plane. The field at each point on the reference plane is taken to have the same amplitude as the field at the corresponding projected point on the radome surface. A phase delay is inserted in each of the parallel rays according to the length of the projection line. While this optical approximation may be quite satisfactory for large, directive antennas, it is likely to introduce excessive error with small antennas.

If the fields are given on an inclined plane (perhaps a plane which is tangential to the radome surface) the far-field pattern can be calculated by an integration over this plane directly without an undue increase in complexity as compared with a preliminary projection to another reference plane. In this way the projection errors are avoided. First, express the fields $E_z(y,z)$ on the inclined reference plane in terms of the amplitude and phase, thus:

$$E_z = |E_z| \, e^{j\alpha}. \tag{3.14}$$

If the fields are assumed to be separable as before, the H-plane far-field pattern associated with E_z is given by eq. 3.7b which can now be written as

$$E_\theta(\phi) = \cos\phi \int |E_z(y)|\, e^{j(\alpha + ky \sin\phi)}\, dy. \qquad (3.15)$$

For numerical evaluation, this integral is approximated by a summation as before, using intervals of length $2y_o$ and using the discrete set of field measurements $E_z(my_o)$ where m is restricted to integral values. A table of $kmy_o \sin\phi$ is first tabulated for the desired values of ϕ and for an adequate range of m. The phase distribution $\alpha(my_o)$ is added to the tabulated values of $kmy_o \sin\phi$, after which the summation is carried out by resolving each term into real and imaginary components and using real addition. Thus, once the function $kmy_o \sin\phi$ has been tabulated, any given amplitude and phase distribution may be used with this computation procedure to determine the corresponding far-field pattern.

Fig. 3.10 illustrates the results obtained with the above procedure using a reference plane tilted 40° from the aperture of the horn shown in Fig. 3.2. The fields of the horn were measured on the reference plane with a dipole probe. A value of 0.25 inch was selected for y_o in the calculations. Similar calculations using reference planes more nearly parallel with the aperture yielded better results. This may indicate that the separability assumption is less valid on planes which are tilted more from the aperture.

The procedure outlined above is useful even with reference planes parallel to the antenna aperture. In the case of asymmetrical antennas it may be preferred to the method described in Section III.2 which is most conveniently used with symmetrical fields.

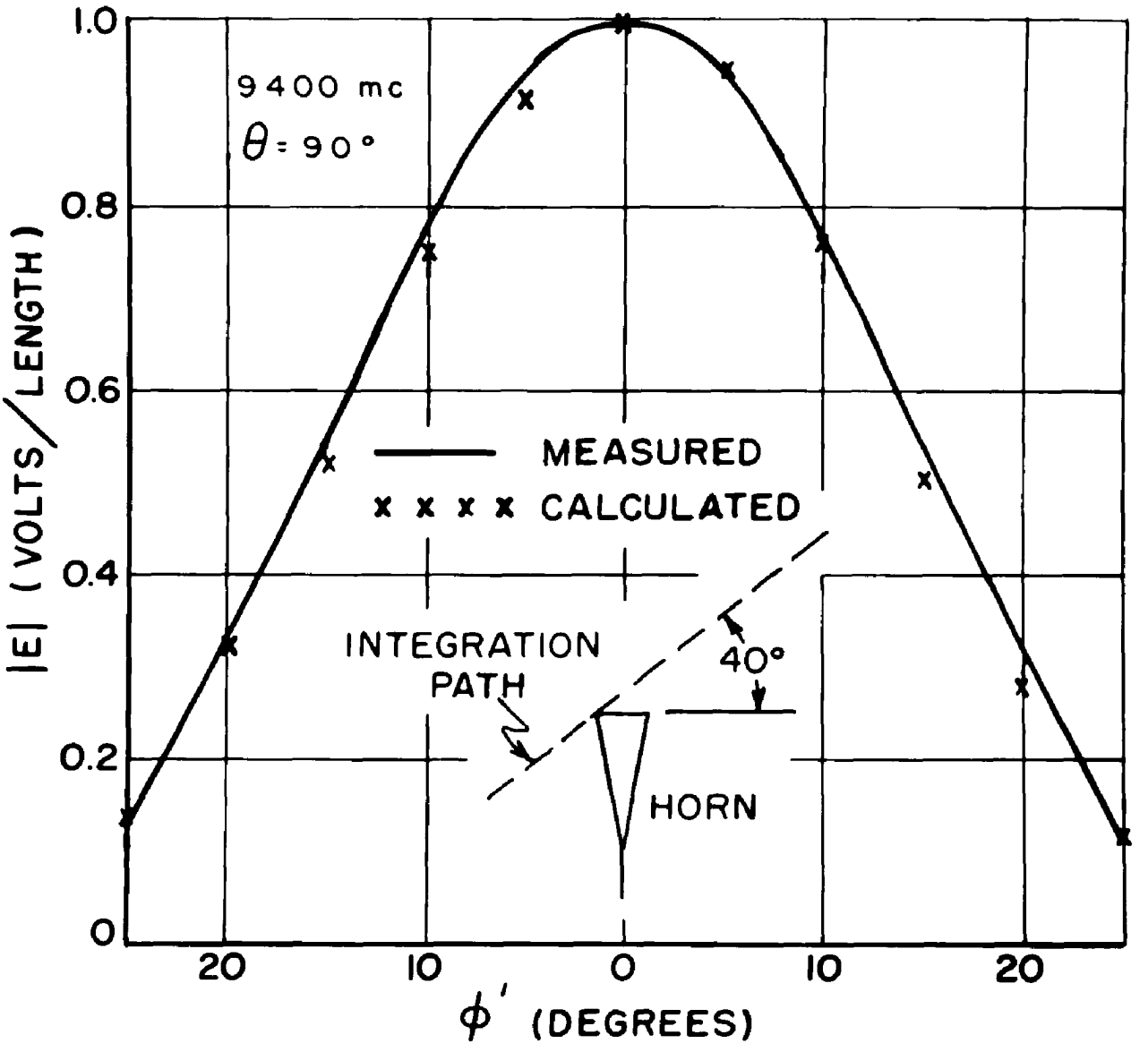

Plate XXIC

Fig. 3.10. Measured and calculated far-field H-plane patterns of horn antenna shown in Fig. 3.2.

5. REFERENCES

1. A. B. Bronwell and R. E. Beam, "Theory and Application of Microwaves", 1st edition, McGraw-Hill Book Co., Inc., New York, 1947, pp. 451-453.

2. V. H. Rumsey, "Huygens Principle for Electromagnetic Waves", Technical Report 444-15, Antenna Laboratory, The Ohio State University Research Foundation; January 25, 1954.

3. S. Silver, "Microwave Antenna Theory and Design", McGraw-Hill Book Co., Inc., New York, 1949, p. 173, equation 8.

4. J. D. Kraus, "Antennas", 1st edition, McGraw-Hill Book Co., Inc., New York, 1950, p. 375.

IV. ANTENNA PATTERN DISTORTION BY DIELECTRIC SHEETS

1. INTRODUCTION

In the design of radomes it is often necessary to calculate the far-field pattern of an antenna covered with a radome. While conventional calculation methods may be adequate when applied to large, well-rounded radomes, better approximations and new techniques are needed for use with small streamlined radomes.

In seeking a better formulation for the problem, one might choose a reference surface inside the radome. It will be shown that in this case a knowledge of the unperturbed antenna fields together with a plane-wave solution for the fields inside the radome are sufficient to determine the radiation pattern. The antenna fields in the absence of a radome are generally available by direct measurement. Thus, if the reference surface is chosen to lie inside the radome it is necessary to analyze transmission through the radome only for plane waves rather than the complicated waves emitted by the antenna. If the radome and antenna were available, the desired patterns could most readily be obtained by direct measurement. However, it is assumed that the radome is in the design stage and is not available for measurements.

2. THEORY

Consider the problem of determining the far-field pattern of antenna 1 shown in Fig. 4.1. Let E_1 and H_1 denote the fields of

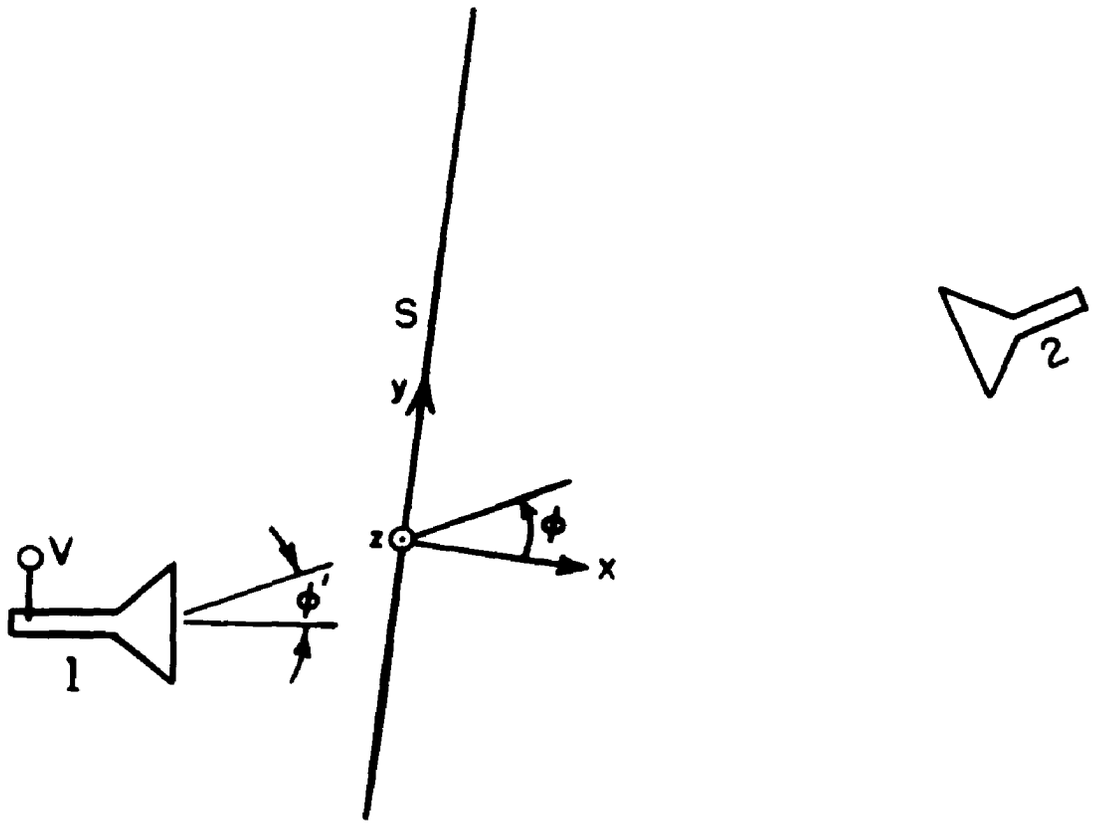

Plate XXIII
Fig. 4.1. Coordinates used in radiation pattern analysis.

antenna 1 when it is functioning as a transmitting antenna. Choose a reference surface S which may be either an infinite plane or a surface which completely encloses antenna 1. In computing the fields of antenna 1 on the source-free side of S, antenna 1 can be replaced by its equivalent electric and magnetic current distributions J_1 and K_1 on S, where

$$J_1 = n_1 \times H_1, \tag{4.1a}$$

and

$$K_1 = E_1 \times n_1, \tag{4.1b}$$

where n_1 is a unit vector in the direction of the outward drawn normal on S. Two vector potentials A and F can now be defined in terms of J_1

and K_1, and the field intensity can be expressed in terms of A and F. If the entire region on the source-free side of S is occupied by a homogeneous medium, the potentials and the electric field intensity are given by eqs. 3.2 and 3.3. These expressions become much more complicated for the case of an inhomogeneous region. Therefore, radome calculations are usually divided into two steps. First, an auxiliary reference plane S" is chosen to pass between antenna 1 and the radome. The fields of antenna 1 on S" are operated on in some fashion to obtain an approximation for the fields on surface S which is outside the radome. Eqs. 3.2 and 3.3 are then used to compute the far-field pattern. This type of analysis, which may be called the conventional approach to the radome problem at present, requires a mathematical description of the transmission of energy from antenna 1 through the radome to the external reference surface.

The problem may be reformulated by introducing a distant transmitting antenna, antenna 2, as in Fig. 4.1. The far-field pattern of antenna 1 is given by the voltage V induced at its terminals as antenna 2 is moved in a circular path centered at antenna 1. Antenna 2 is always aimed at antenna 1 during this circular motion. Let E_2 and H_2 denote the electric and magnetic field intensities on S due to antenna 2 transmitting in the presence of antenna 1. Antenna 2 can be replaced by its equivalent electric and magnetic current distributions J_2 and K_2 on S, where

$$J_2 = n_2 \times H_2, \tag{4.2a}$$

and

$$K_2 = E_2 \times n_2, \tag{4.2b}$$

where n_2 is the unit vector normal to S in the direction of the region occupied by antenna 1. By an application of the Lorentz reciprocal theorem, Kouyoumjian (1) has shown that

$$V = C \iint_S (J_2 \cdot E_1 - K_2 \cdot H_1)\, ds, \tag{4.3}$$

where C is a constant which may be omitted in the calculation of relative far-field patterns. As will be shown, the additional information introduced by the application of the reciprocity theorem makes it possible to simplify the radome analysis by strategic use of eq. 4.3 in place of the conventional approach.

If S is chosen to be a plane, eq. 3.4 may be used to reduce eq. 4.3 to

$$V = \iint_S J_2 \cdot E_1 \, ds = - \iint_S K_2 \cdot H_1 \, ds. \tag{4.4}$$

The constant multiplying factors have been omitted in eq. 4.4, and this will also be done in the remainder of this chapter without further comment, when such factors are of no interest in the problem being considered.

In far-field calculations, antenna 2 is located at a great distance from antenna 1. Then the fields on S due to antenna 2 are plane waves and eq. 4.3 reduces to the usual expression for the far-field pattern of antenna 1 in terms of its aperture fields. For example, if S is chosen to be a plane and if antennas 1 and 2 are linearly polarized in the z-direction, eq. 4.3 yields the H-plane pattern expression given by eq. 3.5b.

To illustrate the application of eq. 4.3 to the radome problem,

consider the far-field pattern of antenna 1 in the presence of an infinite plane dielectric sheet as in Fig. 4.2. Choose as a reference

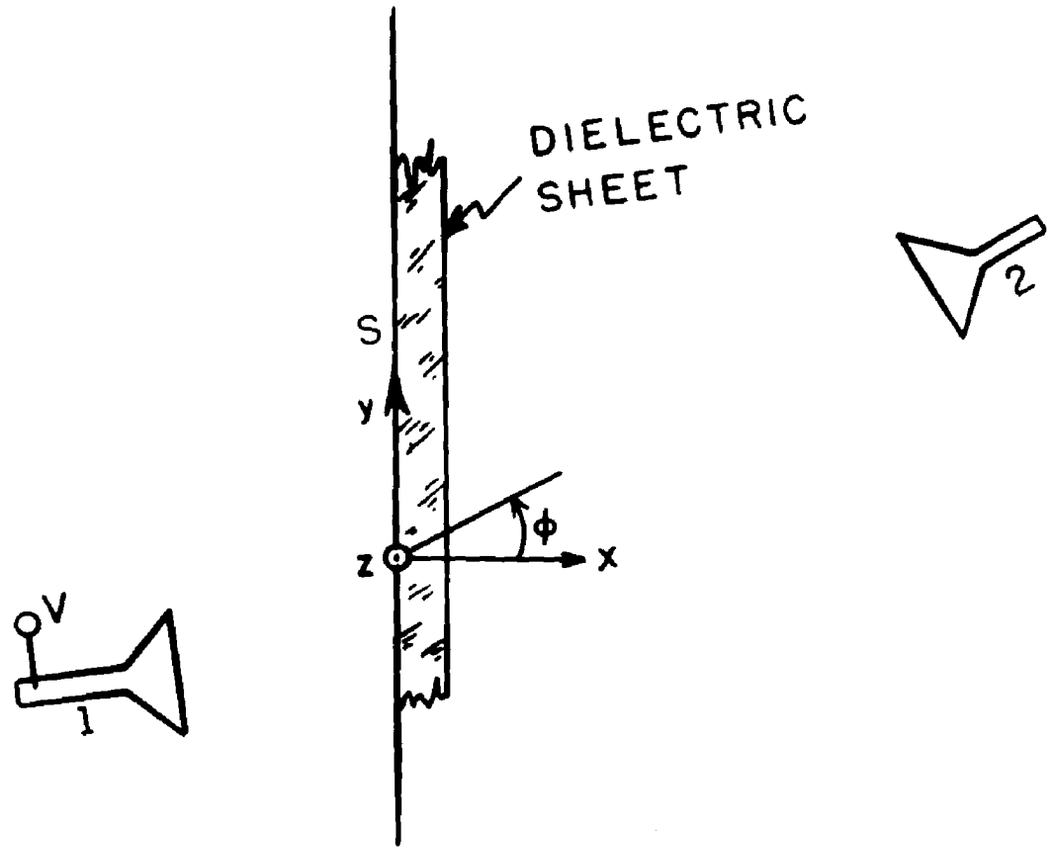

Plate XXIV

Fig. 4.2. Transmission through an infinite plane dielectric sheet.

the surface of the dielectric sheet facing antenna 1. Neglecting reflected waves bouncing back and forth between antenna 1 and the dielectric sheet, the fields of antenna 2 on S are found by employing the plane-wave plane-sheet transmission coefficient T. Using primes to denote quantities in the presence of the dielectric sheet and the absence of primes to denote the corresponding quantities without the dielectric sheet,

$$H_2' = T\,H_2, \tag{4.5a}$$

and

$$J_2' = T\,J_2. \tag{4.5b}$$

From eq. 4.4,

$$V' = \iint J_2' \cdot E_1 \, ds. \tag{4.6}$$

It should be stated that the unperturbed fields E_1 of antenna 1 are correctly employed in eq. 4.6. As a consequence of choosing surface S to pass between antenna 1 and the dielectric sheet it is unnecessary to know the fields of antenna 1 in the presence of the dielectric sheet. From eqs. 4.5 and 4.6, since T is independent of position on S,

$$V' = T \iint_S J_2 \cdot E_1 \, ds = TV. \tag{4.7}$$

That is, knowing the unperturbed far-field pattern V of antenna 1, its pattern V' in the presence of an infinite plane dielectric sheet is found merely by multiplication by the plane-wave plane-sheet transmission coefficient for the polarization and angle of arrival of the plane waves coming from antenna 2. This contrasts with the usual optical approximations in which the transmission coefficient for the angle of incidence of rays from antenna 1 is employed.

Suppose the dielectric surface facing antenna 2 had been chosen as the reference surface. The dielectric sheet would then be considered a part of antenna 1 and it would be necessary to know the fields of antenna 1 on this surface in the presence of the dielectric sheet. Thus, a surface passing between the radome and antenna 1, or perhaps coinciding with the dielectric surface facing antenna 1 is preferred since transmission through a dielectric body is most easily

calculated for plane waves.

Although no actual radome calculations have yet been attempted using these methods, several examples of transmission through infinite plane sheets and finite plane sheets will now be presented.

3. EXAMPLES

Fig. 4.3 shows the measured far-field H-plane patterns of the pyramidal horn of Fig. 3.2 at 9400 mc with a polystyrene (ε=2.53) plane sheet held at an angle of 40° across the horn aperture. The unperturbed pattern is also shown for reference. The calculated points shown in the figure were obtained using eq. 4.7. The dielectric sheet was 0.51 inch thick and was large enough so that its edges were well outside the region illuminated by the horn. The horn has a beam width of 23° to the half-power points. The waves arriving from antenna 2 were polarized perpendicular to the plane of incidence on the dielectric sheet. Hence, the transmission coefficient for perpendicular polarization was employed in the calculations.

Fig. 4.4 shows similar results for the paraboloid of Fig. 3.6 with the same polystyrene sheet at 45°. The paraboloid has a beam width of 23°

One more example using the horn is shown in Fig. 4.5 for a fiberglas sheet having a thickness of 0.382 inch and a dielectric constant of 4.0. This sheet had a lower transmission coefficient than the polystyrene sheet and therefore produced a more pronounced reduction in the far-field amplitude. The fiberglas and polystyrene

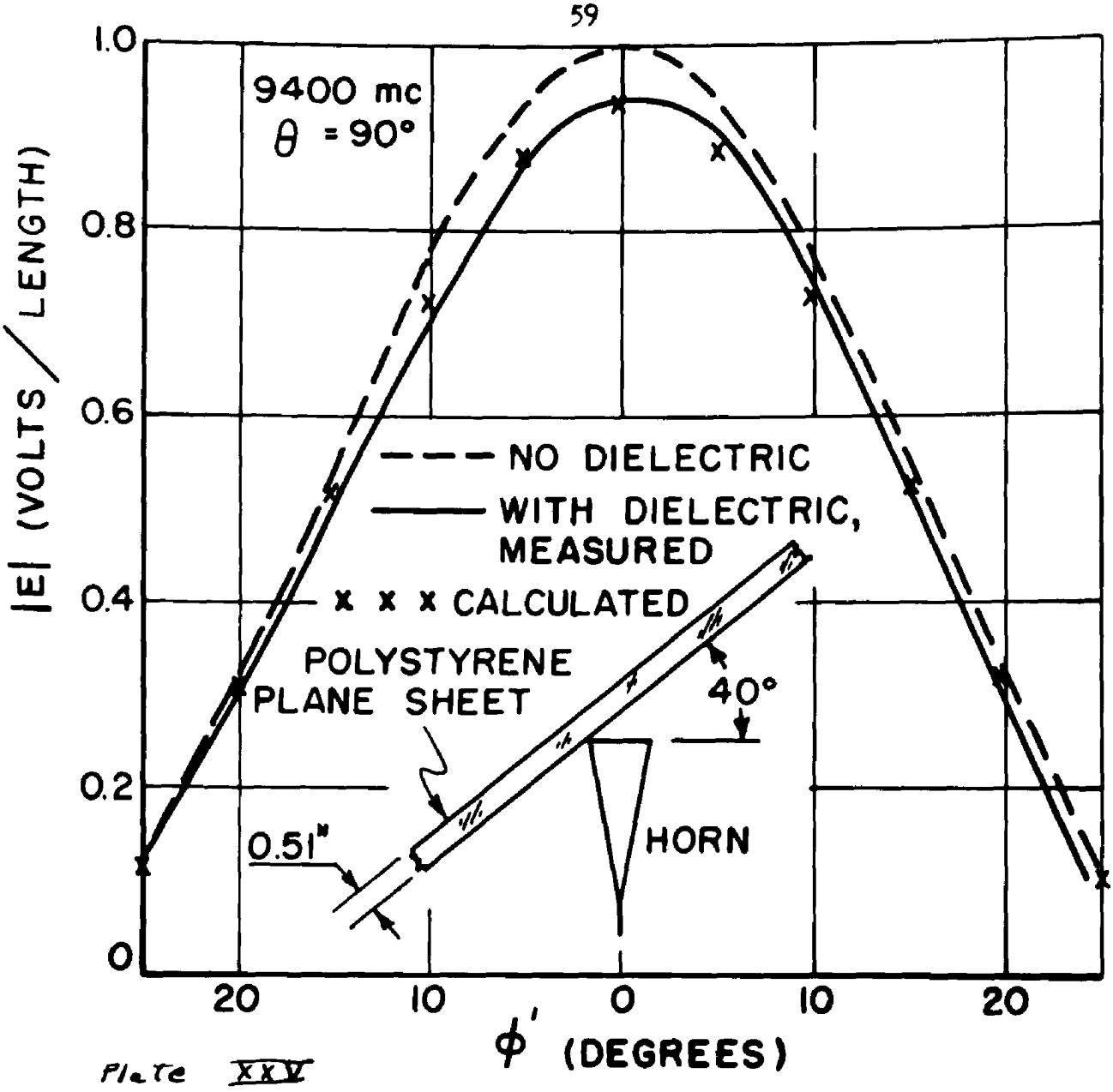

Fig. 4.3. Far-field pattern of horn transmitting through a plane polystyrene sheet.

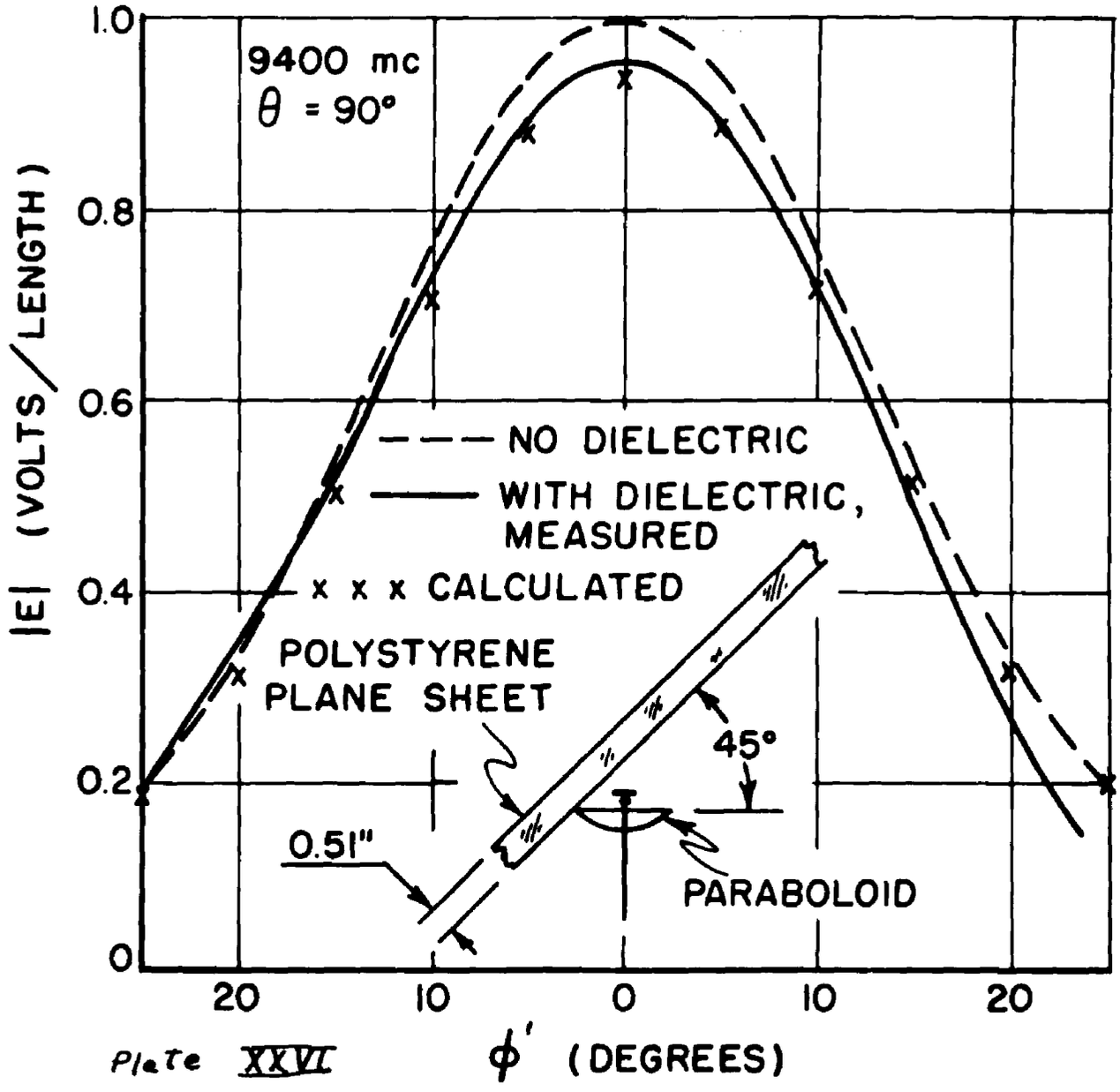

Fig. 4.4. Far-field pattern of paraboloid transmitting through a plane polystyrene sheet.

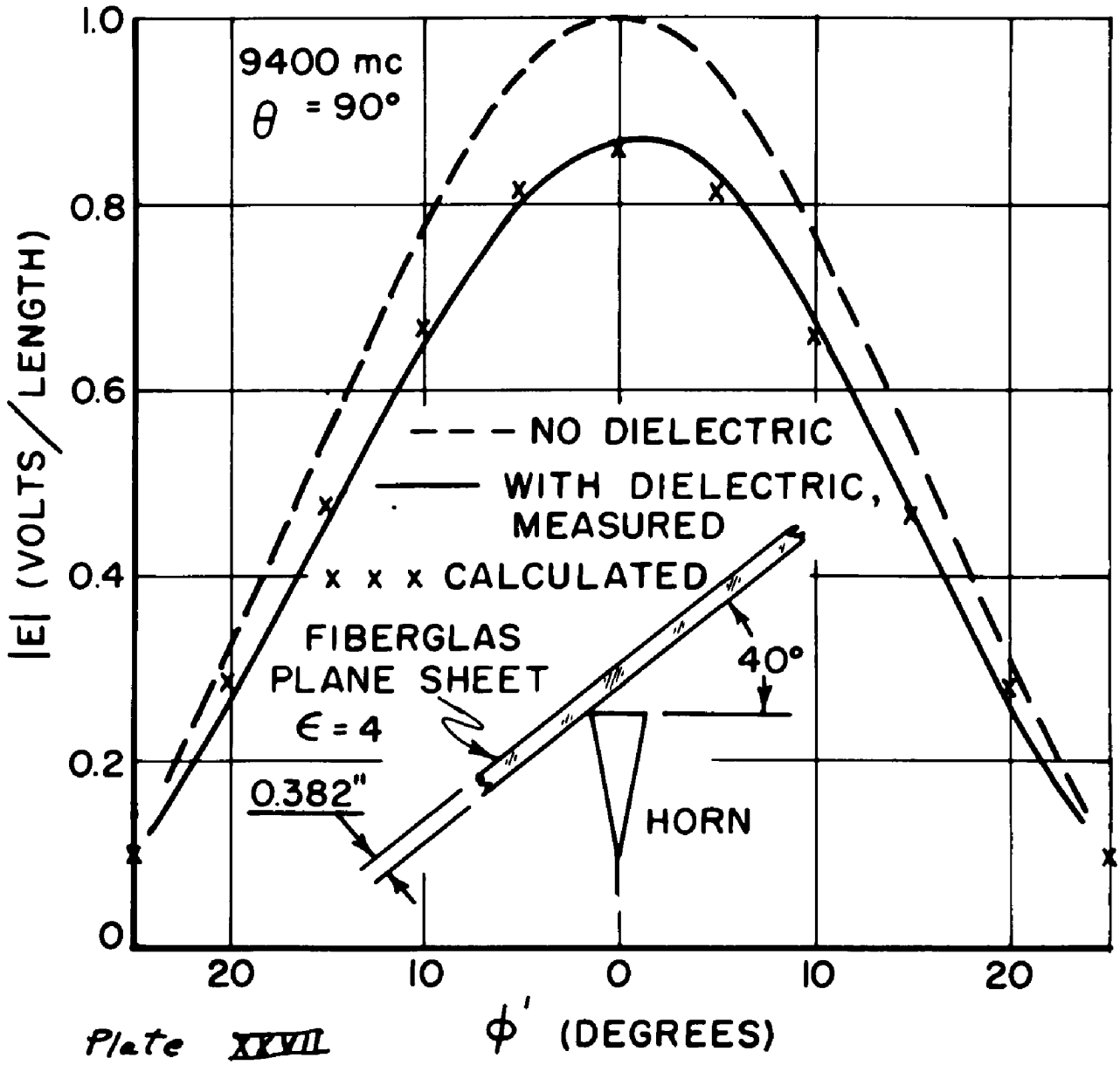

Fig. 4.5. Far-field pattern of horn transmitting through a plane fiberglas sheet.

sheets were each a little over one-half wavelength thick in terms of the wavelength in the dielectric. Any reflected waves bouncing back and forth between the antenna and the dielectric sheet were neglected in the calculations. In many cases this is justified, since radomes usually employ walls of low reflection coefficient.

To get closer to the radome problem, calculations were also carried out for plane dielectric sheets covering only a part of the antenna aperture. A reference surface S was chosen on an infinite plane coinciding with the dielectric surface facing antenna 1. The fields of antenna 1 were measured on S in the absence of the dielectric sheet. Eq. 4.3 requires a knowledge of the fields on S due to antenna 2 radiating in the presence of the dielectric. Although at points remote from the edge of the sheet the fields are given by plane-wave plane-sheet theory, the fields near the edge are more complicated. It is possible that the fields near the edge can be well approximated in terms of an equivalent source located at the edge.

As a first approximation the fields were assumed to be the incident plane wave up to the edge of the dielectric sheet, and were assumed to be given by plane-wave plane-sheet theory on the portion of S covered with dielectric. The numerical integration was carried out using the method described in Section III.4. The results for this approximate calculation are shown in Figs. 4.6 and 4.7 for a polystyrene sheet 0.51 inch thick covering one-half of the horn aperture at angles of 40° and 0°, respectively. It is felt that the agreement between the calculations and measurements is surprisingly

good in view of the simplifying approximations involved. The calculations were carried out on an ordinary desk calculator and required less than one man-day for each far-field pattern.

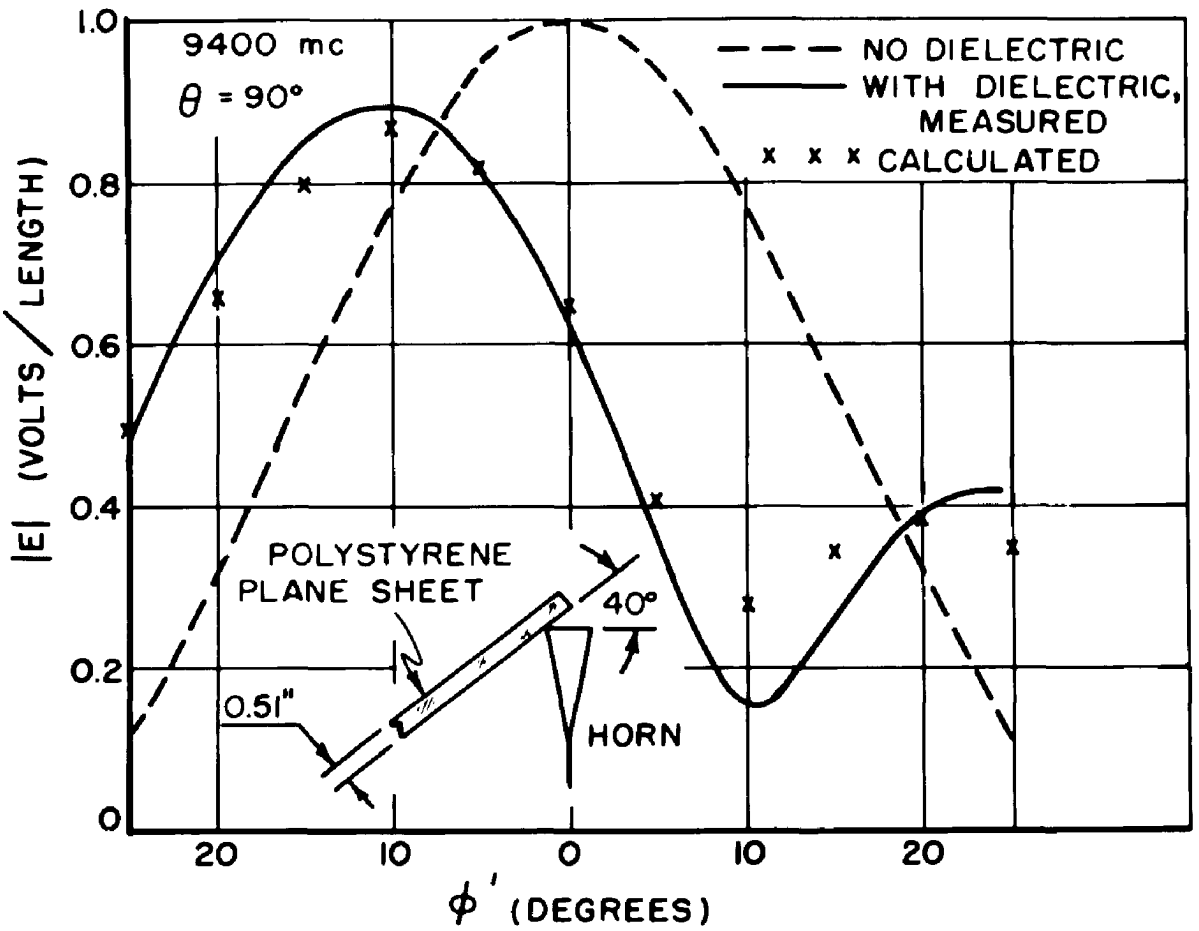

Plate XXVIII

Fig. 4.6. Far-field pattern of horn with aperture partially covered with a plane polystyrene sheet.

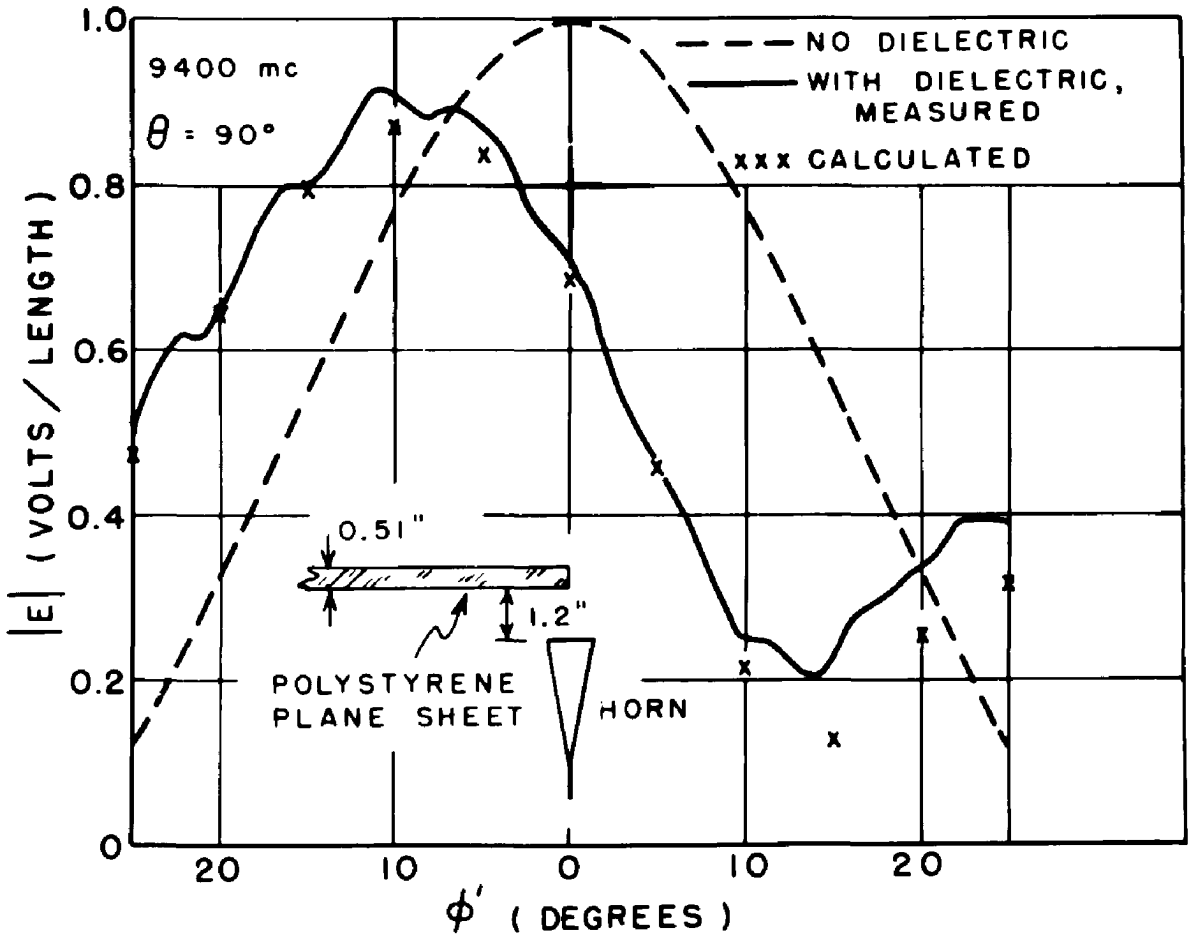

Plate XXIX

Fig. 4.7. Far-field pattern of horn with aperture partially covered with a plane polystyrene sheet.

4. REFERENCES

1. R. G. Kouyoumjian, "The Calculation of the Echo Areas of Perfectly Conducting Objects by the Variational Method", Technical Report 444-13, Antenna Laboratory, The Ohio State University Research Foundation, November 15, 1953, pp. 29 and 80-84.

V. CONCLUSIONS

The properties of the balanced coherent detector are found to be useful in the measurement of microwave fields near a transmitting antenna with and without radome. The sensitivity of such a detector employing bolometers has been measured at 9400 mc and was found to be -125 dbw. This may be contrasted with the sensitivity of -94 dbw which has been measured with a bolometer used as a square-law detector. Crystals perform equally well in the balanced coherent detector, and may be preferred since they require less reference signal power. The high sensitivity available with coherent detection permits the use of smaller, more accurate probes and scatterers in the measurement of field distributions. Balanced coherent detection permits the direct measurement of the time-quadrature components of microwave fields which are found to be convenient in the far-field calculations described in Chapter III.

Electric field distributions can be measured accurately by passing a short metal dipole through the field and recording the wave scattered by the dipole. Ordinarily the method is difficult to apply to radome measurements since the scattered signal is small, critical tuning adjustments are required, and careful attention to stability is necessary. However, by placing a nonlinear impedance at the center of the dipole and applying an audio voltage through slightly conducting threads, the scattered wave can be modulated. It is shown that this technique, together with the use of a balanced

coherent detector, makes it possible to relax the tuning and stability requirements and at the same time to increase the sensitivity of the scattering measurements. As a by-product, this adapts the system to the automatic plotting of phase distributions.

Although the modulated scattering technique has been found to be well suited for radome field measurements, its instrumentation is somewhat more complex than that of direct probing methods. Hence, direct probing may be preferred in cases where it is adequate. The field distribution near a radome was measured with scatterers of various lengths and with several probes. As expected, it was found that the larger probes and scatterers had less resolution and were unable to measure the fine structure in the field distribution. An open-ended waveguide probe was developed which is simple in construction, has an aperture small enough to measure complicated field distributions, and has been found to be sufficiently accurate for many radome near-field measurements.

In radome design it is frequently necessary to calculate the far-field pattern of an antenna covered with a radome, using measured or calculated fields on a surface just outside the radome. Such calculations are lengthy and often require the use of a large computer. The problem is simplified by choosing a plane reference surface. In this case a knowledge of the tangential electric or magnetic fields on the plane is sufficient to determine the far fields. The calculations are further simplified for certain antennas having aperture fields which are, to a good approximation, separable in rectangular

coordinates. This permits the surface integral appearing in the far-field expression to be replaced with a line integration. In the numerical work the line integration is approximated with a summation. It was found that, for the examples which were worked out, the continuous near-field distribution could be replaced with an array of point sources spaced nearly one-half wavelength apart with little loss in accuracy.

In cases where the near fields are symmetrical it is convenient to resolve the complex summation into two real summations, thus minimizing the amount of vector addition involved. The time-quadrature components of the near fields may be measured directly with a balanced coherent detector, thus reducing the numerical work as compared with the usual procedure in which the phase and amplitude distributions are measured. Using these simplifications, far-field patterns can be determined rapidly on a desk calculating machine. Both E-plane and H-plane calculations agree satisfactorily with measured patterns for small horns and paraboloid antennas, as well as for a horn covered with a hollow dielectric wedge. A feature of the method which is important in radome analysis is that it permits rapid evaluation of the far-field distortion associated with any given near-field distortion in any small region in the near field.

A systematic procedure is described for the calculation of far-field patterns based on given near-fields when the reference surface is a plane tilted away from the antenna aperture. In such problems it is common to first project the given fields to a plane which is

parallel with the aperture, and then to compute the far-field pattern by an integration over the new reference plane. The errors introduced by the use of approximate projection methods may be eliminated without undue extra effort by direct integration over the tilted reference plane, using the procedure described in Chapter III.

Conventional methods of radome far-field error calculation are based on optical approximations. It is necessary to mathematically describe the transmission of the complicated antenna fields through the radome to a reference surface outside the radome. An integration over this surface yields the far-field pattern of the antenna with radome. The problem may be reformulated by an application of the reciprocity theorem to express the far-field pattern in terms of an integration over a surface which is most conveniently chosen to pass between the radome and the antenna. In this case the only required data are

(1). the unperturbed fields of the antenna, and

(2). the fields on the reference surface produced by a plane wave incident on the radome from an external source. This simplifies the problem, since transmission through a radome is more easily analyzed for a plane wave than for the complicated waves emitted by the antenna.

A particularly simple result is obtained by this approach for transmission through an infinite plane dielectric sheet inclined at some angle from the antenna aperture. If interaction between the antenna and the sheet is negligible, it is shown that the far-field

pattern with the sheet is merely the unperturbed pattern multiplied by the appropriate plane-wave plane-sheet transmission coefficient. Several examples which are included show that this theory is verified by experimental measurements. The theory is also applied to transmission through a finite plane sheet. In this case, the analysis requires a knowledge of the diffraction field near the edge of the dielectric sheet due to an incident plane wave. Using a simple approximation for the diffraction field, examples are presented which show satisfactory agreement between the theory and experimental measurements. It is felt that these results justify future attempts to apply the theory and techniques to the problems of transmission through curved dielectric sheets and radomes.

AUTOBIOGRAPHY

I, Jack Hubert Richmond, was born in Kalispell, Montana, July 30, 1922. I received my secondary school education in the public schools of Kalispell. My undergraduate training was obtained at Lafayette College, from which I received the degree Bachelor of Science in 1950. From The Ohio State University, I received the degree Master of Science in 1952. In 1952 I received the appointment of Research Associate in the Department of Electrical Engineering at The Ohio State University. I held this position for three years while completing the requirements for the degree Doctor of Philosophy.